Syn-rift carbonate platforms in space and time: testing and refining conceptual models using stratigraphic and seismic numerical forward modelling

Isabella Masiero[a,d], Peter Burgess[a], Cathy Hollis[b], Lucy Manifold[b], Rob Gawthorpe[c], Isabelle Lecomte[c], Jim Marshall[a], Atle Rotevatn[c]

[a] *Quantitative Experimental Stratigraphy Group, Jane Herdman Laboratory, Department of Earth, Ocean and Ecological Science, University of Liverpool, Brownlow Street, Liverpool L69 3GP, U.K.*
[b] *School of Earth, Atmospheric and Environmental Sciences, University of Manchester, Oxford Road, Manchester, M13 9PL, England*
[c] *Department of Earth Science, University of Bergen, P.O.Box 7803, Bergen, N-5020, Norway*
[d] ***Corresponding author, e-mail: isabella.masiero@liverpool.ac.uk***

Abstract: Understanding and predicting architecture and facies distribution of syn-rift carbonates is challenging due to complex control by climatic, tectonic, biological and sedimentological factors. CarboCAT is a three-dimensional stratigraphic forward model of carbonate and mixed carbonate-siliciclastic systems that has recently been developed to include processes controlling carbonate platform development in extensional settings. CarboCAT has been used here to perform numerical experiment investigations of the various processes and factors hypothesised to control syn-rift carbonates sedimentation. Models representing three tectonic scenarios have been calculated and investigated, to characterize facies distribution and architecture of carbonate platforms developed on half-grabens, horsts and transfer zones. For each forward stratigraphic model, forward seismic models have also been calculated, so that modelled stratal geometries presented as

synthetic seismic images can be directly compared with seismic images of subsurface carbonate strata. The CarboCAT models and synthetic seismic images corroborate many elements of the existing syn-rift and early-post-rift conceptual model, but also expand these models by describing how platform architecture and spatial facies distributions vary along strike between hanging-wall, footwall and transfer zone settings. Synthetic seismic images show how platform margins may appear in seismic data, showing significant differences in overall seismic character between prograding and backstepping stacking patterns.

Supplementary material: The digital version of the images included in this paper and the 3D stratigraphic simulation results (ECLIPSE format) can be downloaded from the following repository; `https://www.dropbox.com/sh/q7x4wsi4olv4ilq/AAARZzab3vqeo51GDAm9kVbua?dl=0`. Readers are encouraged to download the supplementary data and visualize the stratigraphic model results in Petrel, to better appreciate the model finer details and 3D nature.

Characterizing and understanding carbonate strata that develop in tectonically active extensional settings is challenging. The architecture and facies distribution of syn-rift carbonates are complex due to the combined influence of climatic, tectonic, biological and sedimentological factors.

Published investigations of these controlling factors have been based on both subsurface and outcrop data (e.g. Bosence, 2012; Dorobek, 2008; Cross and Bosence, 2008; Wilson et al., 2000; Rosales, 1999; Bosence et al., 1998;

Rosales et al., 1994; Burchette, 1988; Leeder and Gawthorpe, 1987). However, these mostly qualitative models are limited by incomplete datasets, are often subjective and in some cases difficult to falsify, all of which limits how much they can reveal of potentially complex interaction of multiple controls in such highly dynamic systems. To begin to address this complexity, a complementary numerical modelling approach is useful (e.g. Williams et al., 2011; Wilson et al., 2000; Bosence et al., 1998) but rather than developing general tectono-stratigraphic models, modelling-based investigations often address specific case studies. For example, Wilson et al. (2000) combine elements of *Carbonate* and *Domino* (described by Bosence et al., 1998) to determine if observed geometries of the Tonasa Platform (SE Asia) might have been dominantly controlled by tectonic processes. In addition, numerical models used in these studies are essentially 2D and dip-oriented, often with simple fault models that cannot address along-strike platform variability and the 3D nature of certain processes such as sediment transport.

To address these limitations and progress understanding of syn-rift and early post-rift carbonate platforms, we present here the results of the first study using a comprehensive set of 3D stratigraphic and seismic forward models to investigate how various processes and parameters control carbonate strata development of active fault block carbonate platforms, and the resulting seismic appearance. A large number of simulations have been performed, representing carbonate growth on the most common structural elements occurring in extensional basins, namely horsts, half-grabens and transfer zones. For each of these settings, the most influential controls on carbonate growth have been identified from literature, quantified, and tested. The selected

model parameters aim to represent the variety of possible syn-rift tectono-sedimentary scenarios for tropical carbonate platforms (*sensu* Bosence, 2005) of the type interpreted to occur in the Miocene of Suez Rift (e.g. Cross and Bosence, 2008; Bosence et al., 1998; Burchette, 1988; Leeder and Gawthorpe, 1987), the Miocene in Indonesia (e.g. Mayal et al., 1990) or the Carboniferous of Northern England (e.g. Gutteridge, 1987, 1984; Manifol et al., 2020; Manifold, 2019). We have investigated how different combinations of parameters affect platform development in three-dimensions, illustrating along-strike variability of facies and platform margin geometries and stacking patterns.

Model formulation, initial conditions and parameters

CarboCAT (Masiero et al., 2020; Burgess, 2013) is a three-dimensional stratigraphic forward model of carbonate and mixed carbonate-siliciclastic systems. It includes multiple sedimentary, climatic and tectonic processes, and is capable of reproducing the complex, three-dimensional facies heterogeneity characterizing carbonate platform strata (Masiero et al., 2020). CarboCAT has been used here to generate a series of three-dimensional tectono-sedimentary models representing syn-rift carbonate systems. Three structural scenarios have been investigated, to characterize facies distribution and architecture of carbonate platforms developed on half-grabens, horst and transfer zones during 2.5 My of fault activity and 0.5 My of post-rift quiescence. Each model run has a 3 My duration, with a calculation time step of 1 ky and a chronostratigraphic surface stored every 1 ky. Climatic, sedimen-

tary and structural model parameters have been selected for each structural configuration, to represent five base-case generic syn-tectonic platform scenarios (Table 1). These five scenarios investigate carbonate platform response to the different controls in three dimensions. To characterize the seismic appearance of these tectono-stratigraphic models, we have used a depth-domain 3D-convolution approach, integrating both illumination and resolution effects (Lecomte et al., 2015; Lecomte, 2008), to develop synthetic seismic images from CarboCAT facies models. Input parameters and variables used in the model runs and synthetic seismic calculations are listed in Table 1, 2 and 3, and discussed below.

Structural model and initial bathymetry

CarboCAT requires definition of an initial bathymetry on which carbonate deposition begins. For these experiments, we have developed a larger-scale tectonic scenario (Figure 1), representing a significant portion of an idealized extensional basin that includes various structural elements. Carbonate growth has then been simulated on selected sub-sections of this bigger area. Since timing of platform initiation in extensional basins is variable, initial bathymetries for our model runs may represent an early-rift setting (Figure 1(a-b-f-h)), or a more mature stage where significant fault displacement has already occurred (Figure 1(c-d-g)). Tectonic processes implemented in CarboCAT include: i) constant-rate regional subsidence affecting the entire model area (specified in Table 1), and ii) fault controlled spatially and temporally variable subsidence, controlled by input parameters that determine footwall and hanging-wall deformation rates, fault angle, and initial and final length of the fault segment (see Masiero et al., 2020, Fig. 2).

Carbonate factories

Model simulations include three in-situ carbonate factories, one coarse grained, high-energy margin facies (e.g. coralgal reef), and two finer grained platform interior facies (e.g. packstone and wackestone). The two platform interior lithologies ensure development of facies heterogeneity, as observed in most carbonate systems. Production rate of each factory, and the relative proportion of transportable sediment, are listed in Table 1, constrained by modern observations for reef margin and platform interior facies (e.g. Schlager, 2000, 1981). In CarboCAT, in-situ facies are defined by input parameters controlling spatial distribution, production rate, and the proportion of produced sediment available for re-redistribution by transport mechanisms. Spatial facies distribution is controlled by a cellular automata algorithm, while the accumulation rate in each model cell is calculated from a production-rate-versus-depth curve (e.g. Bosscher and Schlager, 1992) that can be different for each carbonate facies type. Facies occurrence is also controlled by wave energy, limiting facies deposition to areas where wave energy is within specified maximum and minimum values. The values of energy used in these model runs are consistent with measurements of wave energy across a reef fringed platform area (e.g. Péquignet et al., 2011). Platform margin facies require wave energy to be larger than $4 \cdot 10^4 J\ m^{-2}$, while a lower value is needed for platform interior strata.

Sediment erosion, transport, and deposition can occur by current-driven or gravity-driven mechanisms. Hemipelagic sediment is generated from the erosion of fine grained facies (i.e. Platform Interior 2) and transported exclusively by currents as suspended load. Redistribution of coarser-grained facies

(i.e. Reef and Platform Interior 1) can be either current driven as bedload or gravity driven. Deposition of fine-grained pelagic sediment occurs at a maximum rate of 80 $m \cdot My^{-1}$ (see Enos, 1991) and decreases with decreasing water depth. Deposition of pelagic sediment occurs only in deep waters where wave energy and current velocity are zero.

Climatic conditions

CarboCAT simulates various environmental controls on carbonate platform growth using eustatic sea-level curves with a range of oscillation amplitudes and frequencies, and various wind directions and magnitudes.

Sea-level - To evaluate glacioeustatic control on fault-block carbonate platforms a sea-level curve is applied *Model run 2-22-62-65* and *32* with a 50 meter amplitude and 1 My period oscillation (e.g. Miller et al., 2005), resulting in a $\sim 0.1\ mm{\cdot}y^{-1}$ rate of fall that exceeds tectonic subsidence rates. Mechanisms for eustatic oscillations with this period are poorly understood (Miall, 2010) but during icehouse intervals at least, could be driven by long-term changes in ice sheet volume.

Wind - Wind direction sub-parallel to the main structural direction has been observed in various extensional systems (e.g. Gulf Of Suez; Roberts and Murray, 1984). In the widely studied Suez Rift, this preferential wind direction appears to lead to reef occurrence on the windward side of relatively small, sub-rounded platforms (e.g. Ashrafi platform; Roberts and Murray, 1984) while, on larger-scale fault-block platforms, elongated reef build-ups preferentially develop along-strike, on fault blocks facing the open marine environment (Perrin et al., 1998). This may be a consequence of the capacity of large structures to influence water hydrodynamics (already argued

by Purkis et al., 2012), for example by wave refraction while approaching the footwall crest over a dipping fault plane. Since faults with large displacements can only be vertical in CarboCAT, refraction in this setting does not occur, so the best approximation for half-graben and horst structures includes wind blowing perpendicular to the fault strike. Conversely, wind direction in relay-ramp structures is set at 45 degrees to the fault strike, developing high energy conditions on both the footwall crests and the transfer zone.

Seismic model

Acoustic properties used to populate the geological model and develop the synthetic seismic are listed in Table 3, and are derived from several sources (e.g. Fournier et al., 2014; Anselmetti and Eberli, 1993) with the assumption that the modelled coarse and fine-grained facies should generate acoustic impedance contrasts. Seismic models include layered overburden composed of alternating shale and sandstone layers and, since siliciclastic deposition usually characterizes the early-rift stages (e.g. Red Sea; Purser et al., 1998), underlying strata are sandstones. The synthetic seismic results are presented in a red and blue coloured seismic display, where a decrease in acoustic impedance is represented by a blue trough.

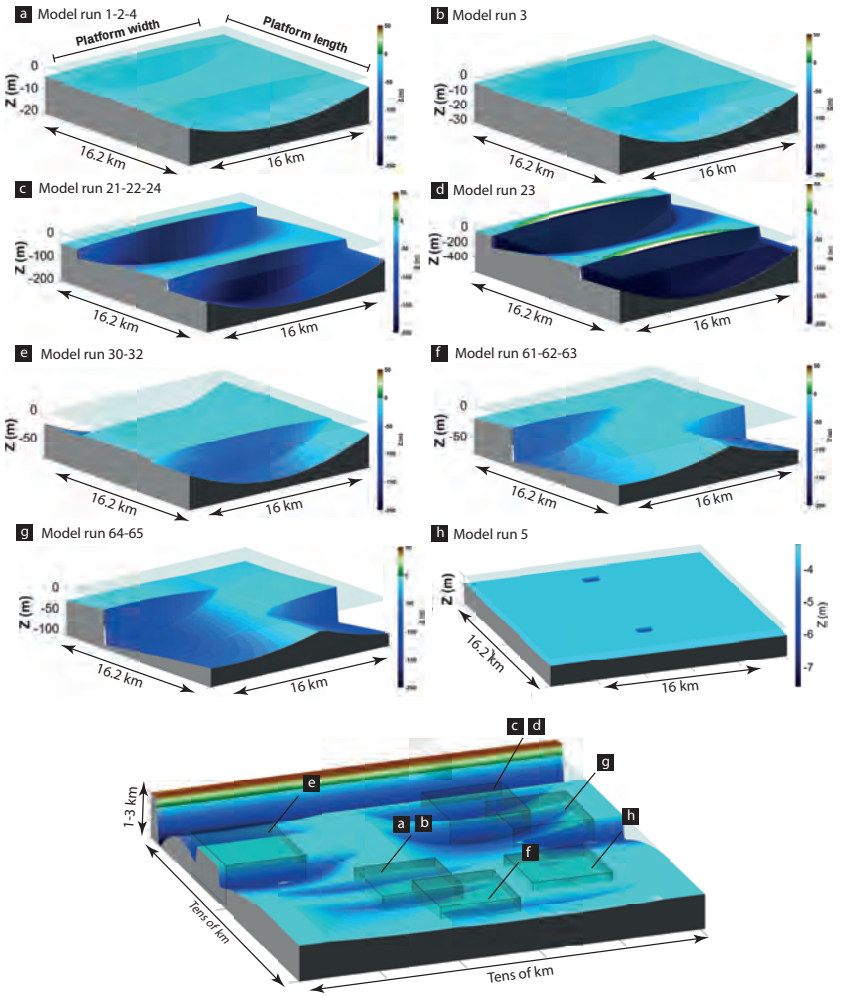

Figure 1: Initial bathymetries of all Model runs (a-h) showing their positions in an idealized extensional basin. Faults are visible as steeply inclined surfaces across which there is a sudden increase in bathymetry.

Table 1: *Variable parameters used in model runs. In bold: parameters varied from the relative base model.*

Model	**Wind direction**	**Slip rate** ($mm \cdot y^{-1}$)	**Regional subsidence rate** ($mm \cdot y^{-1}$)	**Production rates** ($mm \cdot y^{-1}$)	**Transport rates (%)**	**Sea-level oscillation**	**Siliciclastic input**
Half-graben platform with high carbonate accumulation/transport ratio and low slope build-up ability (Model run 1-5) and transfer zones (Model run 61-63)							
Model run 1 (base model)	Footwall facing wind	0.6	0.2	Reef = 3000; Platf. Int. 1-2 = 1800	Reef = 50; Platf. Int. 1-2 = 65	SL = 0;	No
Model run 2	Footwall facing wind	0.6	0.2	Reef = 3000; Platf. Int. 1-2 = 1800	Reef = 50; Platf. Int. 1-2 = 65	**Amplitude = 50 m; Cycle = 1 My**	No
Model run 3	Footwall facing wind	**2.64**	0.2	Reef = 3000; Platf. Int. 1-2 = 1800	Reef = 50; Platf. Int. 1-2 = 65	SL = 0;	No
Model run 4	**Hanging-wall facing wind**	0.6	0.2	Reef = 3000; Platf. Int. 1-2 = 1800	Reef = 50; Platf. Int. 1-2 = 65	SL = 0;	No
Model run 5	Footwall facing wind	0.6	0.2	Reef = 3000; Platf. Int. 1-2 = 1800	Reef = 50; Platf. Int. 1-2 = 65	SL = 0;	No
Model run 61 (base model)	Footwall facing wind	0.6	0.2	Reef = 3000; Platf. Int. 1-2 = 1800	Reef = 50; Platf. Int. 1-2 = 65	SL = 0;	No
Model run 62	Footwall facing wind	0.6	0.2	Reef = 3000; Platf. Int. 1-2 = 1800	Reef = 50; Platf. Int. 1-2 = 65	**Amplitude = 50 m; Cycle = 1 My**	No
Model run 63	Footwall facing wind	0.6	0.2	Reef = 3000; Platf. Int. 1-2 = 1800	Reef = 50; Platf. Int. 1-2 = 65	SL = 0;	**Yes**

Table 1: *Continued.*

Model	**Wind direction**	**Slip rate** ($mm \cdot y^{-1}$)	**Regional subsidence rate** ($mm \cdot y^{-1}$)	**Production rates** ($mm \cdot y^{-1}$)	**Transport rates (%)**	**Sea-level oscillation**	**Siliciclastic input**
Half-graben platform with low carbonate accumulation/transport ratio and high slope build-up ability (Model run 21-24) and transfer zones (Model run 64-65)							
Model run 21 (base model)	Footwall facing wind	0.25	0.06	Reef = 4500; Platf. Int. 1-2 = 3500	Reef = 80; Platf. Int. 1-2 = 90	SL = 0;	No
Model run 22	Footwall facing wind	0.25	0.06	Reef = 4500; Platf. Int. 1-2 = 3500	Reef = 80; Platf. Int. 1-2 = 90	**Amplitude = 50 m; Cycle = 1 My**	No
Model run 23	Footwall facing wind	**0.9**	0.06	Reef = 4500; Platf. Int. 1-2 = 3500	Reef = 80; Platf. Int. 1-2 = 90	SL = 0;	No
Model run 24	**Hanging-wall facing wind**	0.25	0.06	Reef = 4500; Platf. Int. 1-2 = 3500	Reef = 80; Platf. Int. 1-2 = 90	SL = 0;	No
Model run 64 (base model)	Footwall facing wind	0.25	0.06	Reef = 4500; Platf. Int. 1-2 = 3500	Reef = 80; Platf. Int. 1-2 = 90	SL = 0;	No
Model run 65	Footwall facing wind	0.25	0.06	Reef = 4500; Platf. Int. 1-2 = 3500	Reef = 80; Platf. Int. 1-2 = 90	**Amplitude = 50 m; Cycle = 1 My**	No
Horst platform							
Model run 30 (base model)	Toward -y	0.6	0.2	Reef = 3000; Platf. Int. 1-2 = 1800	Reef = 50; Platf. Int. 1-2 = 65	SL = 0;	No
Model run 32	Toward -y	0.6	0.2	Reef = 3000; Platf. Int. 1-2 = 1800	Reef = 50; Platf. Int. 1-2 = 65	**Amplitude = 50 m; Cycle = 1 My**	No

Table 2: *General, structural and environmental input parameters with specified literature sources, used in all the model runs.*

Parameters	**Values**	**Reasonale and references**
Run time	3 My	Reasonable observation period for the modelled scenarios.
Time step	1000 yr	Trade-off between model resolution and run time.
Cell size	200 m	Trade-off between model resolution and run time.
Model area	16 x 16.2 km^2	Reasonable scale for the represented structural scenarios.
Structural parameters		
Fault activity	2.5 My	Reasonable observation period, allowing the modelled faults to develop significant displacement accordingly to realistic slip rates.
Post-rift quiescence	0.5 My	Reasonable observation period, allowing deposition of significant thickness of post-rift carbonate strata.
Fault dip	90°	Value recommended in Carbo-CAT to avoid artefacts when faults have displacements exceeding cell size.
Initial fault length	16 km	Carbonate deposition in extensional settings usually begins after an initial siliciclastic phase (e.g. Red Sea; Purser et al., 1998)
Final fault length	25 km	Fault length is calculated in agreement with displacement/length relationship proposed by Cowie and Scholz (1992).
Environmental parameters		
Wind velocity	18 $m\ s^{-1}$	Beaufort scale (near-gale).
Wave period in deep water	8 s	Observed ocean wave periods lie between 3 and 20 s (e.g. Mandlier and Kench, 2012; Péquignet et al., 2011)
Wave base	-80 m	Common value reported in literature.
Fetch length outside model boundary	4 km	Distance from the subsequent structural high.
Grain size threshold between suspended/bedload transport	0.09 mm	Consistent with the grain size of the carbonate in-situ factories such as one of them generates hemipelagic sediments.
Lower boundary for wave-induced current	-80 m	Consistent with the wave base boundary.

Table 3: *Acoustic properties of modelled carbonate lithologies.*

Rock type/Facies	**Density** ($g \cdot cm^{-3}$)	**P-wave velocity** ($m \cdot s^{-1}$)
Reef and derived current deposit	2.53	4688
Interior 1 and derived current deposit	2.74	5996
Interior 2 and derived hemipelagic	2.78	6000
Gravity flow deposits	2.67	5259
Siliciclastic sandstone	2.4	3000
Pelagic	2.8	6283
Shale	2.4	2600

Results

Half-graben

Half-grabens are the most common structural configuration in syn-rift settings. Carbonate strata are influenced by footwall uplift and coeval hanging-wall subsidence (Jackson and McKenzie, 1988; Stein and Barrientos, 1985), generating fault block rotation around an idealized fulcrum (Ravnås and Steel, 1998; Leeder and Gawthorpe, 1987), consequent relative sea-level falls on the footwall crest, and relative sea-level rise on the hanging-wall dip slope. Our modelling results (Figure 2, 3, 4, 5, 6 and 7) suggest that platform development near the footwall margin is primarily controlled by slip rate and how it changes along-strike. Hanging-wall dip-slope-margin geometry and stacking patterns are mainly controlled by the ratio between carbonate accumulation and transport rates, with some influence from fault slip rates affecting platform margin migration rates.

High carbonate in-situ accumulation/transport ratio and low slope build-up ability

Base model - Model run 1 has a subsidence rate of 200 $m \cdot My^{-1}$, slip rate equal to 0.6 $mm \cdot y^{-1}$, high carbonate sediment accumulation/transport ratio, and marine incursion during the early-rift stage (Figure 2 a-c). These parameters generate aggradation and backstepping of the hanging-wall dip-slope margin, progressively reducing down-dip platform length. Backstepping rate decreases from $\sim$18 $mm \cdot y^{-1}$ to zero as fault rotation increases, driving platform morphology to evolve from a homoclinal ramp into a steep-sided, aggradational flat-top platform. Synsedimentary fault tilting increases

accommodation down-dip, forming a growth-wedge geometry (see Figure 2 b and Figure 3 a), contrasted with sub-parallel layers deposited during the last 0.5 million years of post-rift quiescence. Fault-truncated carbonate strata develop on the footwall margin. Prevalent wind direction toward the footwall crest generates windward-leeward facies variability. Reefal build-ups develop on the wind-facing footwall crest, and low-energy platform interior facies dominate the leeward hanging-wall dip-slope platform. The hanging-wall basin is filled with hemipelagic sediments, intercalated with pelagic strata and gravity flow deposits, derived from the hanging-wall platform and the footwall crest of the adjacent half-graben. In-situ carbonates occur in the deepest part of the basin (Figure 2 b), originally deposited on a relatively flat platform top but then drowned, subsided and buried by hanging-wall strata. The thickness of these in-situ carbonate strata increased toward fault tip points (Figure 2 a), due to decreasing displacement rate that progressively delays drowning and backstepping. Similarly, footwall margin strata thickness increases laterally, due to decreasing footwall uplift. Overall platform thickness increases from the uplifted footwall crest down dip, due to increasing accommodation, and then decreases again, where water depth inhibits carbonate production (Figure 3 a).

Platform interior strata are characterized seismically by relatively continuous, medium-to-high-amplitude reflections with a 60-85 m vertical spacing (Figure 2 c). Locally, low amplitude, acoustically sub-transparent areas characterize more homogeneous strata. Reflection geometry is sub-parallel, locally mounded and divergent toward the hanging-wall dip slope. Platform margin reef strata are also lithologically homogeneous and therefore acous-

tically transparent. The base carbonate surface is imaged by a continuous, high-amplitude negative reflection, resulting from strong acoustic impedance contrast between carbonates and underlying sandstones. In contrast, the top carbonate reflection is laterally variable in amplitude and polarity, reflecting the underlying carbonate facies heterogeneity.

Eustatic control - Model run 2 has input parameters set as in *Model run 1*, but also a 1 My cycle sea-level curve with 50 meters amplitude (Figure 2 d-g). Three stratigraphic sequences (S1, S2 and S3 in Figure 2 e) are generated, showing an overall transgressive stacking pattern (Figure 2 d). In each stratigraphic sequence, falling-stage (FSST) and lowstand (LSST) system tracts are characterized by development of a subaerial platform top and deposition of offlapping platform interior strata, moving carbonate factories down-dip in a forced regressive regime (Figure 2 f). Increasing hanging-wall subsidence progressively reduces down-dip extension of subaerial exposure surfaces from S1 to S3 (Figure 2 e). During transgressions, the hanging-wall dip-slope margin backsteps and reef strata are deposited on the footwall crest. During highstands, a thin sequence of platform interior strata is deposited on the reef margin, generating a strong negative reflection, resulting from the lithological contrast between platform interior strata and underlying reef. This reflection defines a platform top sequence boundary, and continues down-dip, where it marks the transition between pelagic and underlying platform interior strata. Hanging-wall sedimentation is dominantly pelagic when sea-level fall exposes the footwall-crest, shutting down shallow-water benthic carbonate factories. Conversely, hanging-wall strata are dominantly resedimented grainy deposits during transgression and highstand. System

tracts thickness and down-dip extension vary along-strike, due to varying displacement and footwall uplift rates, with most prolonged subaerial exposure and unconfomities on the footwall crests (see Figure 2 e and Figure 3 b).

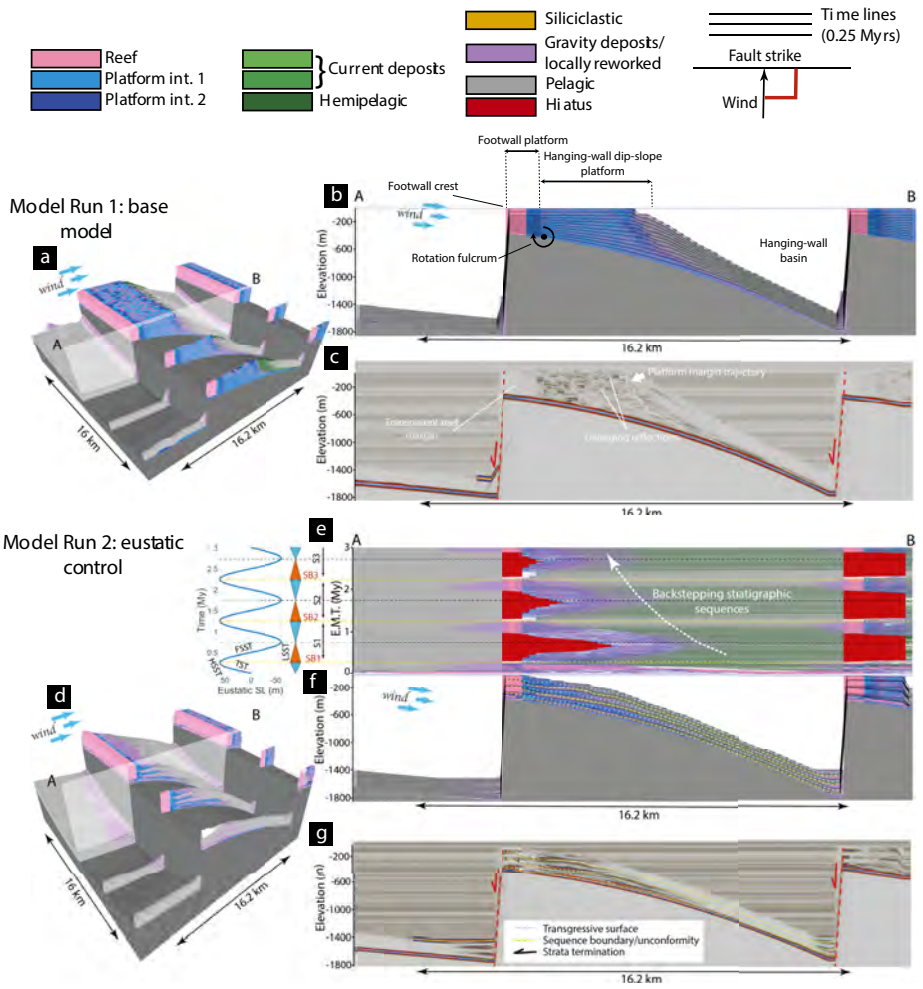

Figure 2 *(previous page)*: Results of *Model run 1-2* showing a sliced 3D view of the models (a and d), a dip-oriented cross-section through each model (b and f), equivalent seismic images of the same cross-section (c and g) and (e), a single chronostratigraphic diagram of the cross-section from *Model run 2*, to show the development of unconformities caused by eustatic sea-level oscillations. Note how the backstepping stacking pattern characterizing the hangingwall margin of *Model run 1* is retained in the overall stratigraphic sequences stacking pattern of *Model run 2*.

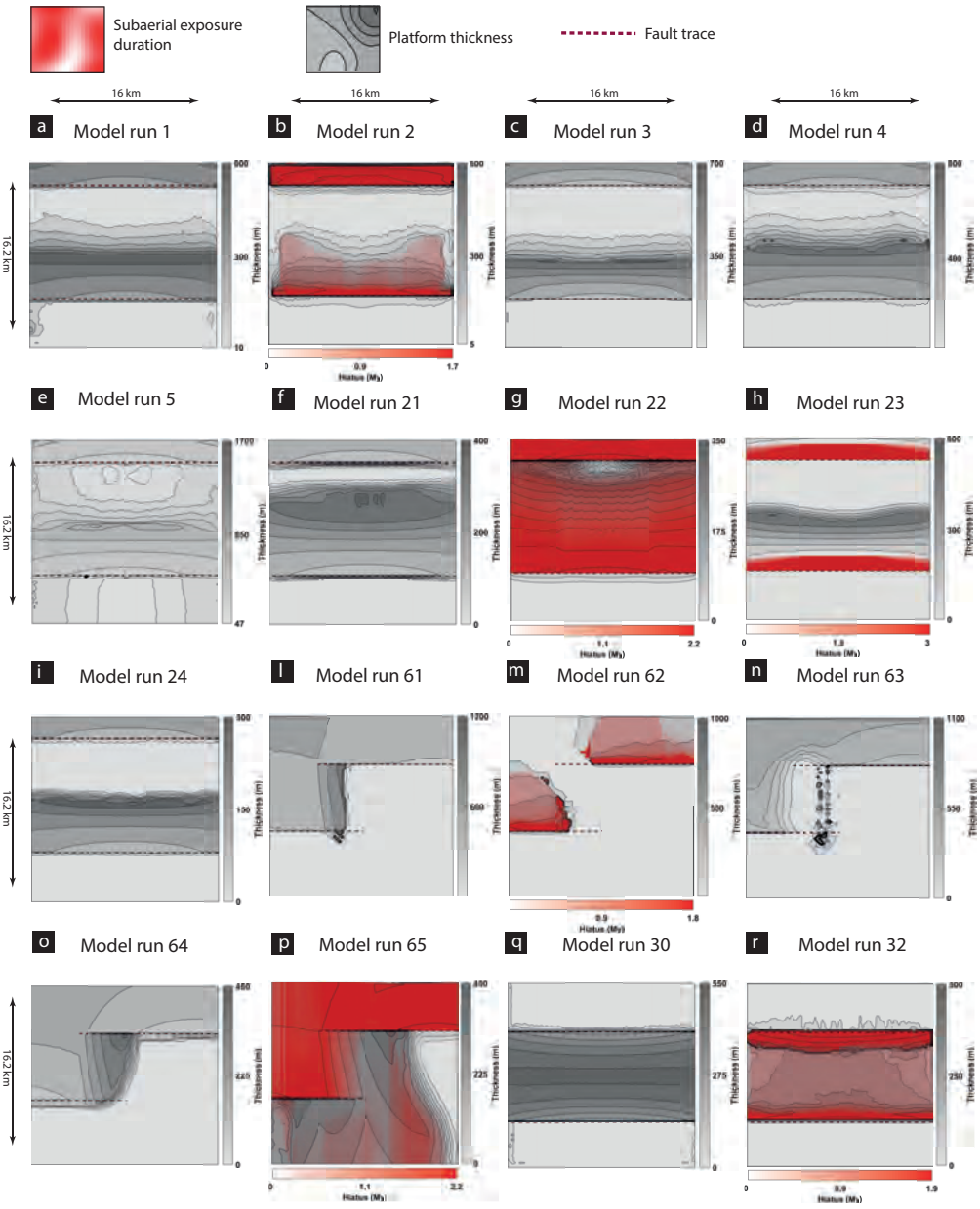
Subaerial exposure duration
Platform thickness
Fault trace
16 km
a Model run 1
b Model run 2
c Model run 3
d Model run 4
16.2 km
e Model run 5
f Model run 21
g Model run 22
h Model run 23
i Model run 24
l Model run 61
m Model run 62
n Model run 63
o Model run 64
p Model run 65
q Model run 30
r Model run 32
Thickness (m)
Hiatus (Ma)

Figure 3 *(previous page)*: Platform thickness (hemipelagic and pelagic sediments are excluded) and duration of subaerial exposure events. It is important to notice the difference between the tectonic-derived subaerial exposure (*Model run 23*), limited to the footwall crest, and those generated by eustatic sea-level fall (*Model run 2* and *Model run 22*) extending into the hanging-wall dip-slope.

Displacement rate - *Model run 3* (Figure 4 a-c) has similar input parameters to *Model run 1* but fault slip rates have been increased from 0.6 $mm \cdot y^{-1}$ to 1.2 $mm \cdot y^{-1}$. Platform transition from a ramp into an aggradational flat-topped steep-margin platform occurs within the first million years, driven by the fault block rotation that accelerates development of a break in slope. Hangingwall basin subsidence also limits the areal extent of shallow water carbonate production, while footwall uplift reduces accommodation.

Wind direction - In *Model run 4* (Figure 4 d-f) the wind is blowing in the opposite direction to *Model run 1*. The hanging-wall platform margin is now windward, yet the reef factory only finally colonizes the margin during the post-rift phase. The footwall margin shows sub-parallel, low amplitude reflections and the hanging-wall platform margin is imaged by higher frequency and amplitude reflections, generated by pelagic and gravity flows alternate deposition, lacking hemipelagic.

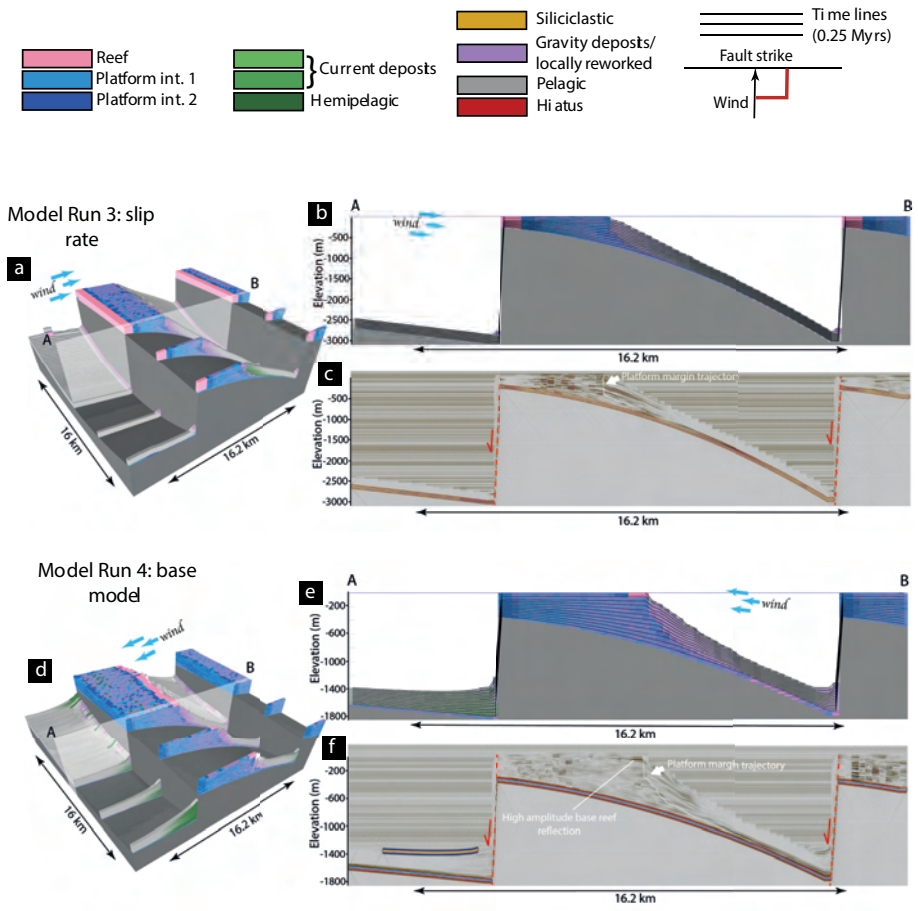
Reef
Platform int. 1
Platform int. 2
Current deposits
Hemipelagic
Siliciclastic
Gravity deposits/ locally reworked
Pelagic
Hiatus
Time lines (0.25 Myrs)
Fault strike
Wind
Model Run 3: slip rate
a
b
c
wind
A
B
16 km
16.2 km
Elevation (m)
-500
-1000
-1500
-2000
-2500
-3000
16.2 km
Platform margin trajectory
Model Run 4: base model
d
e
f
-200
-600
-1000
-1400
-1800
High amplitude base reef reflection

Figure 4 *(previous page)*: Results of *Model run 3-4* showing a sliced 3D view of the models (a and d), a dip-oriented cross-section through each model (b and e), equivalent seismic images of the same cross-section (c and f). Note how the high rate of hangingwall basin subsidence limits the areal extent of shallow water carbonate production in *Model run 3*.

Fault nucleation - In *Model run 5* (Figure 5 a-c) the initial length of the fault segment is reduced to 1 km from the 16 km of *Model run 1* to simulate fault segmentation of pre-existing carbonate strata. Because the fault grows laterally from the central point, the center of the footwall crest is colonized by a reef factory for the entire model duration but the base of the reef strata become progressively younger, and the reef strata thickness decreases towards the fault tips.

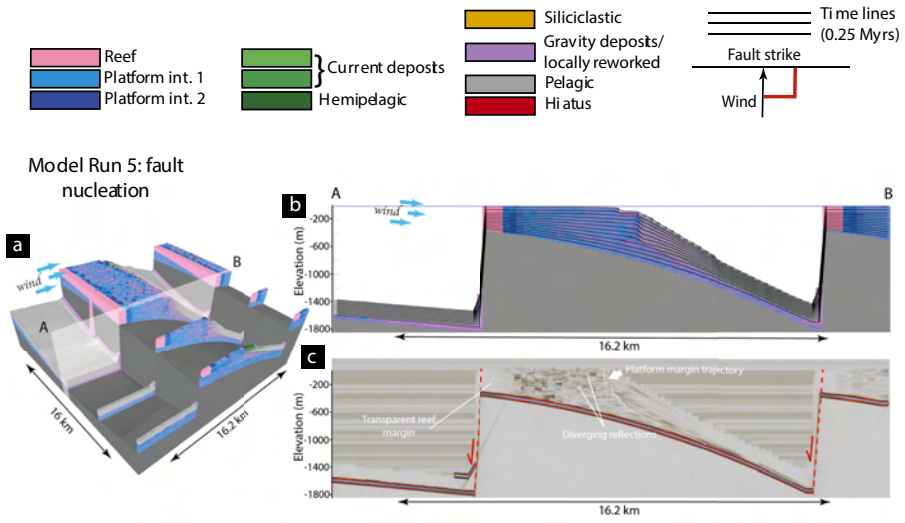

Figure 5: Results of *Model run 5* showing a sliced 3D view of the models (a), a dip-oriented cross-section (b), equivalent seismic images of the same cross-section (c). Note the along-strike thickness variation of the reef strata.

Low carbonate in-situ accumulation/transport ratio and high slope build-up ability

Base model - *Model run 21* has 60 $m \cdot My^{-1}$ regional subsidence, 0.3 $mm \cdot y^{-1}$ slip-rate, low carbonate sediment accumulation/transport ratio

and system flooding during late-rift stage (Figure 6 a-c). The hanging-wall dip-slope margin progrades basinward with a rate that decreases from $\sim$3 $mm \cdot y^{-1}$ to zero as fault rotation increases, generating more pronounced dip-slope stratal thickening (Figure 3 f). Meanwhile, aggradation rate increases, and platform morphology evolves from a distally steepened ramp into flat-top and steep margin. During this phase, aggradation prevails (Figure 6 b). The carbonate platform nucleates on a highly rotated fault block, under high sea-level (see Figure 1 c). During this 'start-up' phase carbonate platform develops relatively isolated build-ups on a dipping surface under high wave-energy conditions. Abundant local and basinward carbonate resedimentation is generated by both tectonic shedding (*sensu* Playton and Kerans, 2002) and highstand shedding (e.g. Schlager et al., 1994). Fault displacement rate decreases toward fault tip points and basin bathymetry also decreases accordingly. The hanging-wall dip-slope margin includes a depositional slope, generated by gravity flow deposits gradually passing down-dip into hemipelagic and pelagic facies. In seismic this hanging-wall margin slope is characterized by acoustic transparency generated by lithologically uniform and steep grainy deposits (Figure 6 c). During post-rift quiescence hanging-wall dip-slope platform margin progradation restarts, generating a high amplitude event overlying the relative transparent slope facies (Figure 6 b-c).

Eustatic control - Model run 22 has parameters set as in *Model run 21*, but a 1 My cycle sea-level curve with 50 meters maximum amplitude is applied (Figure 6 d-g). Stratigraphic sequences S1, S2 and S3 prograde basinward, to the point where carbonate platforms developed on adjacent half-grabens

merge into each other (Figure 6 d). Therefore, platform length progressively increases and the platform area subaerially exposed during sea-level fall and lowstand, increases accordingly (Figure 6 e). During this stage, the hanging-wall dip-slope margin progrades and downsteps, developing offlapping geometries (Figure 6 f-g). The transgressive system tract is characterized by hanging-wall dip-slope margin aggradation and platform interior strata onlapping the transgressive surface (Figure 6 f-g). Platform interior strata are deposited on the reef margin during highstand, generating high-amplitude troughs. Within the seismic model, three high-amplitude peaks mark the transgressive surface, generated by contrast between platform margin deposition on older grainy foresets during forced regression.

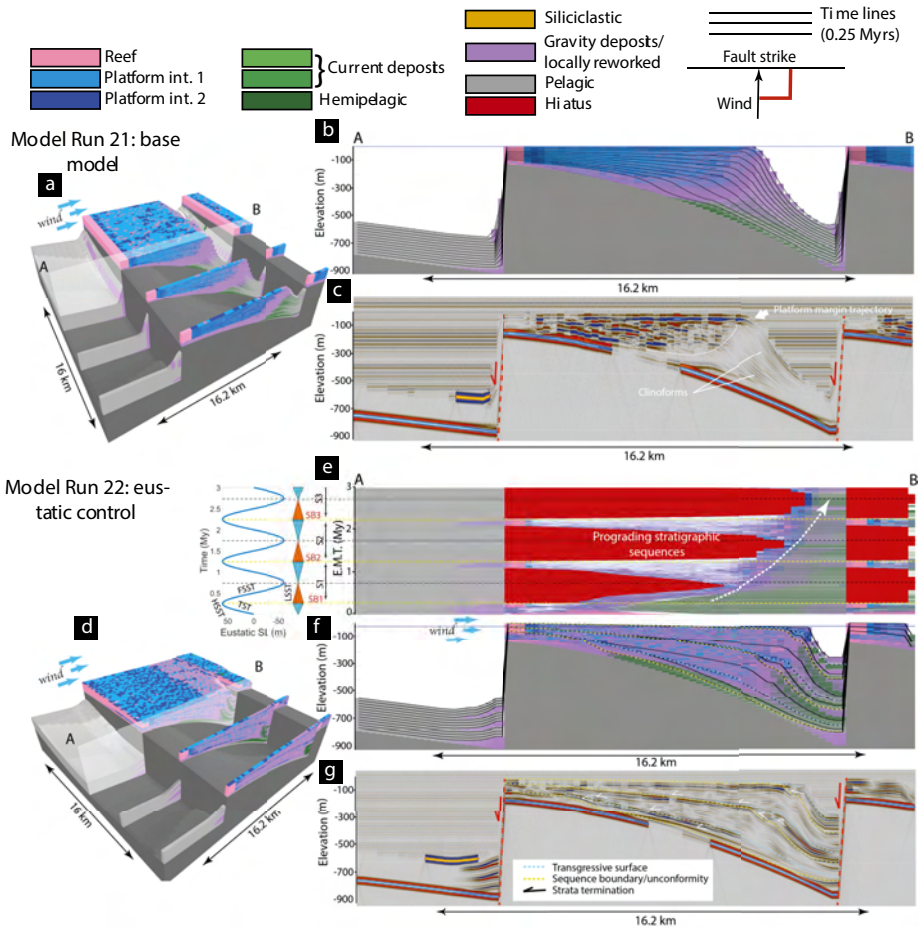
Reef
Platform int. 1
Platform int. 2
Current deposits
Hemipelagic
Siliciclastic
Gravity deposits/ locally reworked
Pelagic
Hiatus
Time lines (0.25 Myrs)
Fault strike
Wind
Model Run 21: base model
a
b
c
wind
A
B
16 km
16.2 km
Elevation (m)
-100
-300
-500
-700
-900
Platform margin trajectory
Clinoforms
Model Run 22: eustatic control
d
e
f
g
SB3
SB2
SB1
Time (My)
Eustatic SL (m)
HSST
FSST
TST
LST
E.M.T. (My)
Prograding stratigraphic sequences
Transgressive surface
Sequence boundary/unconformity
Strata termination

Figure 6 *(previous page)*: Results of *Model run 21-22* showing a sliced 3D view of the models (a and d), a dip-oriented cross-section through each model (b and f), equivalent seismic images of the same cross-section (c and g) and (e), a single chronostratigraphic diagram of the cross-section from *Model run 21*, to show the development of unconformities caused by eustatic sea-level oscillations. Note the progressive increasing extent of subaerial exposure surfaces in *Model run 22* sequences, generated by low subsidence rate and high transport rates, generating sequences overall progradation and basin overfilling.

Slip rate - In *Model run 23* (Figure 7 a-d) fault displacement rate has been increased from 0.3 $mm \cdot y^{-1}$ of *Model run 21* to 1 $mm \cdot y^{-1}$. A narrow carbonate platform results, fringing the central subaerially exposed footwall crest. The tectonically generated exposure surfaces develop only up-dip of the fault rotation fulcrum (Figure 3 h). On the hanging-wall dip-slope margin aggradation prevails because of a reduced progradation rate. Pelagic strata dominate the hanging-wall basin, and sediment supply from the distal carbonate platform is absent.

Windward hanging-wall dip-slope margin - (Figure 7 e-g) shows the results of *Model run 24* with the wind blowing in the opposite direction compared to *Model run 21*. The resulting hanging-wall dip-slope margin is dominated by reef strata through the entire model duration. Margin progradation is limited to the first million years, prior to development of an aggradational steep margin that enhances platform margin vertical growth. In seismic, the reef dominated hanging-wall margin is characterized by high-amplitude reflection events generated by the lithological contrast between porous reef strata and tight platform interior sediment that occur due to local, small-scale interfingering of the two lithologies.

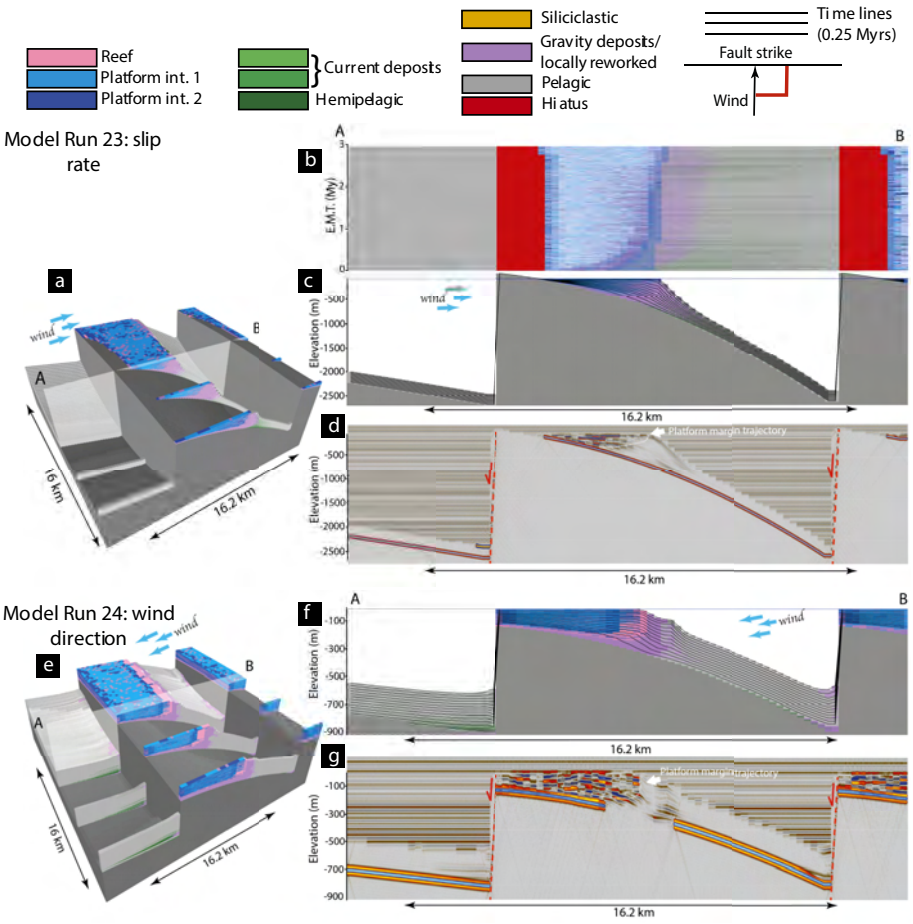
Reef
Platform int. 1
Platform int. 2
Current deposits
Hemipelagic
Siliciclastic
Gravity deposits/ locally reworked
Pelagic
Hiatus
Time lines (0.25 Myrs)
Fault strike
Wind
Model Run 23: slip rate
Model Run 24: wind direction
a
b
c
d
e
f
g
A
B
wind
16 km
16.2 km
E.M.T. (My)
Elevation (m)
Platform margin trajectory

Figure 7 *(previous page)*: Results of *Model run 23-24* showing a sliced 3D view of the models (a, e), a dip-oriented cross-section through each model (c and f), equivalent seismic images of the same cross-section (d and g) and (b), a single chronostratigraphic diagram of the cross-section from *Model run 23*, to show the development of unconformities caused by coseismic footwall uplift exceeding regional subsidence under constant eustatic sea-level. It is important to notice that a relatively high slip rate (*Model run 23*) generates a small, fringing platform rather than affecting the margin stacking, which is still prograding, albeit at a lower rate. Conversely, the high production rates of the reef facies (*Model run 24*) lead to margin aggradation.

Transfer zone carbonate platforms

Transfer zones are important structural elements that transfer displacement between individual faults or basin segments (Morley et al., 1990; Rosendahl, 1987; Rosendahl et al., 1986). Transfer zones influence basin drainage and strata, routing sediments into the rift basin (Gawthorpe and Hurst, 1993) and, when siliclastic influx is low or episodic, becoming sites of in-situ carbonate deposition (e.g. Loza Espejel et al., 2019; Cross and Bosence, 2008; Bosworth et al., 1998). CarboCAT modelling results (Figure 8, 9 and 10) suggest that sedimentation on transfer zones shows significant similarities with hanging-wall dip-slopes. However, the high production rates of the reef factory promote platform margin aggradational stacking.

Transfer zone margin between half-grabens with high carbonate in-situ accumulation/transport ratio and low slope build-up ability

Base model - Model run 61 (Figure 8 a-c) simulates development of a carbonate platform on a relay ramp connecting the hanging wall and footwall of two en-echelon faults, using structural and sedimentary parameters of *Model run 1* as well as a 45 degree wind direction. Sedimentation on the relay ramp includes platform interior strata, thickening toward the hanging wall basin, and a predominantly aggrading reefal margin. Gravity flow deposits are also abundant. Increased fault-segment linkage progressively subsides and rotates sub-horizontal, thin carbonate strata that were originally deposited on the hanging-wall block (Figure 8 b). This abrupt thinning of relay ramp strata is not adequately resolved in the synthetic seismic section (Figure 8 c) where the thinning is imaged as apparent onlap terminations.

Eustatic control - Model run 62 has input parameters set as in *Model run 61* but a generic sea-level curve with 1 My cycle and amplitude of 50 m (Figure 8 e) is used (Figure 8 d-g). Despite the eustatic oscillations, high reef factory production rates lead to keep-up aggradation on the relay ramp platform margin (Figure 8 f). During the first transgressive event, a ramp-type platform with a distally steepened margin is generated. Carbonate accumulation is outpaced by sea-level rise, limiting platform margin aggradation. The lack of a platform margin allows development of high energy conditions in the platform interior, where reef-build ups develop, prior to deepening during high-stand. A platform margin barrier reef also develops, along with deposition of more typical platform interior strata (Figure 8 f). During the falling stage (FSST) and low-stand (LSST) of S1, the platform top is subaerially exposed, carbonate production is shifted down-dip on the relay-ramp, where thin reef and platform interior strata are deposited (Figure 8 e-f). During the following highstand (S2), the platform interior drowns and pelagic strata are subsequently deposited in a deep lagoon. During the S2 sea-level fall and lowstand only the uplifted reef margin is subaerially exposed, and inner platform accommodation controls deposition of platform interior strata (Figure 8 f). The final transgression is associated with almost complete drowning of the platform interior, carbonate production is limited to the reef margin, and a deep lagoon ($\sim$150 m) develops, filled with pelagic sediment and minor re-deposited material from the uplifted margin (Figure 8 f). This relatively homogeneous lithology generates a high-amplitude, well-defined negative platform top reflection (Figure 8 g).

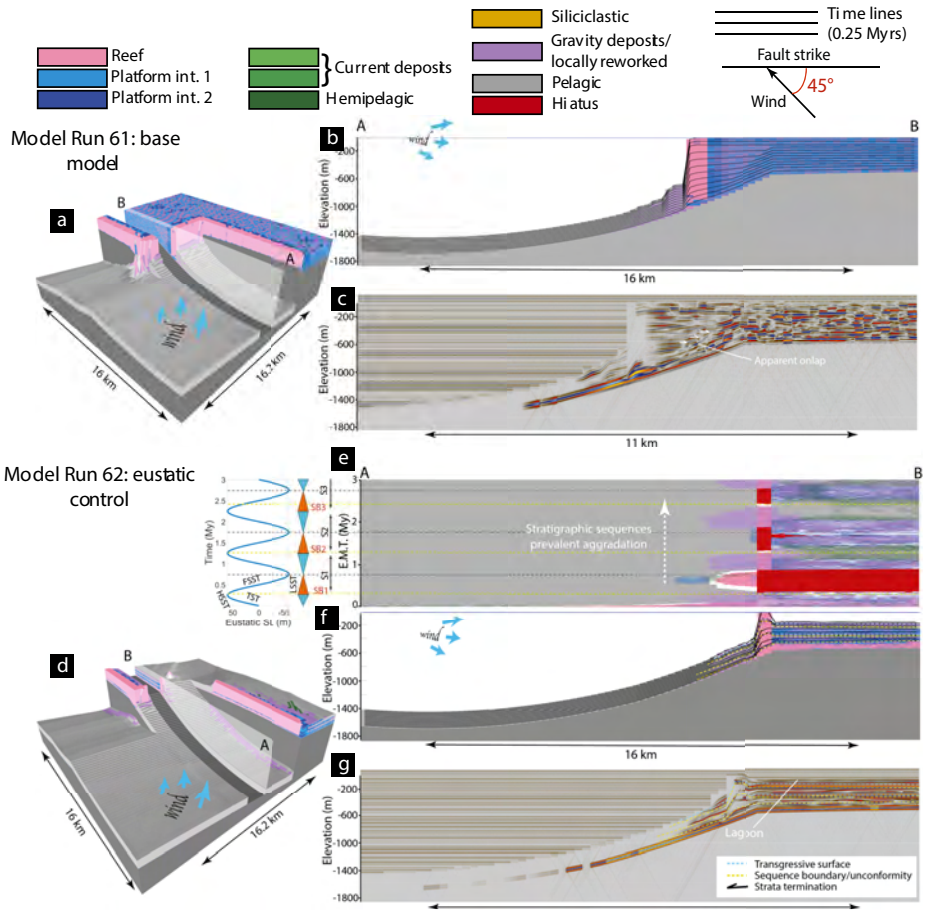
Reef
Platform int. 1
Platform int. 2
Current deposits
Hemipelagic
Siliciclastic
Gravity deposits/ locally reworked
Pelagic
Hiatus
Time lines (0.25 Myrs)
Fault strike
45°
Wind
Model Run 61: base model
Model Run 62: eustatic control
a
b
c
d
e
f
g
16 km
16.2 km
11 km
Apparent onlap
Stratigraphic sequences prevalent aggradation
Lagoon
Transgressive surface
Sequence boundary/unconformity
Strata termination
Elevation (m)
E.M.T. (My)
Time (My)
Eustatic SL (m)
SB3
SB2
SB1
FSST
LSST
TST

Figure 8 *(previous page)*: Results of *Model run 61-62* showing a sliced 3D view of the models (a, d), a dip-oriented cross-section through each model (b, f), equivalent seismic images of the same cross-section (c, g), and (e), chronostratigraphic diagram of the cross-section from *Model run 62*, to show the development of unconformities caused by eustatic sea-level fall.

Land attached - Model run 63 (Figure 9 a-c) has input parameters in agreement with *Model run 61*. In addition, periodically varying volume of siliciclastic sediment is introduced to the transfer zone area, to simulate development of a fan-delta. This results in almost complete suppression of in-situ carbonate production on the relay ramp, which accumulates only localized reef build-ups and associated re-sedimented deposits, developed during phases of low siliciclastic input. However, siliciclastic sediments do maintain shallow water depths, suitable for reef growth. In synthetic seismic section (Figure 9 c), isolated reef build-up tops and bottoms are marked by sub-horizontal, respectively negative and positive reflections, associated with sigmoidal reflections generated by adjacent re-sedimented grainy deposits.

Transfer zone margin between half-grabens with low carbonate in-situ accumulation/transport ratio and high slope build-up ability

Base model - Model run 64 (Figure 10 a-c) has input parameters as in *Model run 21*. This results in initial progradation of the transfer zone platform margin, followed by dominant aggradation (Figure 10 b-c). Seismically, the platform margin is well-defined by sigmoidal packages of high-amplitude reflections generated by lithological contrast between reef, platform interior facies, and grainy slope strata (Figure 10 c).

Eustatic control - Model run 65 (Figure 10 d-g) has input parameters

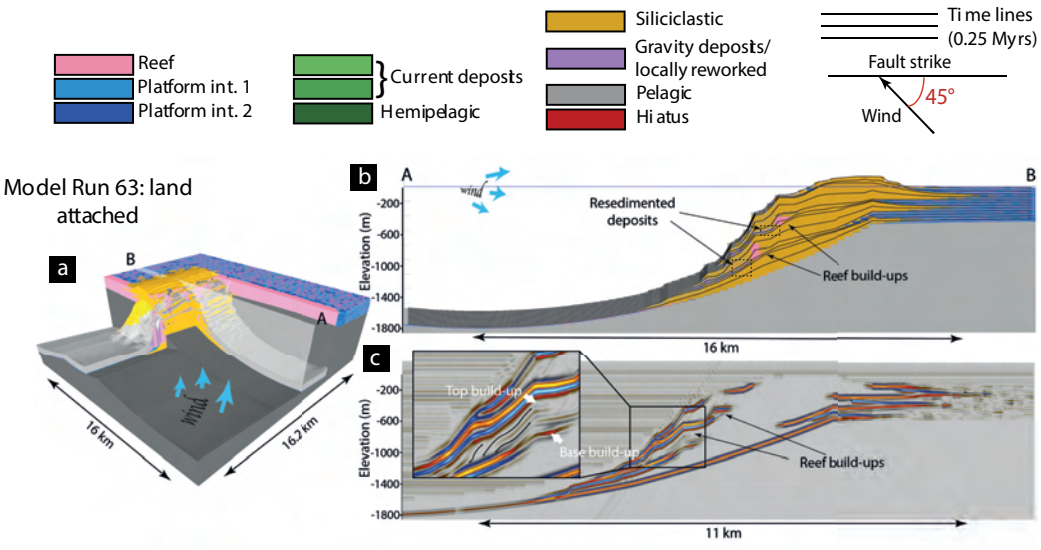

Figure 9: Results of *Model run 63* showing a sliced 3D view of the model (a), a dip-oriented cross-section (b), equivalent seismic image of the same cross-section (c).

as *Model run 64* but periodic sea-level change (Figure10 e). The generated stratigraphic sequences S1, S2 and S3 prograde basinward. Progradation occurs mostly during sea-level falls and lowstands, when the carbonate factory migrates basinward, generating falling-stage offlapping geometries on the relay ramp (Figure 10 f). Sea-level fall exceeds subsidence on the relay ramp, and the platform top is subaerially exposed (Figure 10 e). Conversely, during transgressive and high-stand events, margin aggradation prevails. During this phase, limited platform top accommodation leads to the deposition of a package of thin strata. In the seismic image, the top of the reefal margin is identified by a positive, high-amplitude reflection (Figure 10 g).

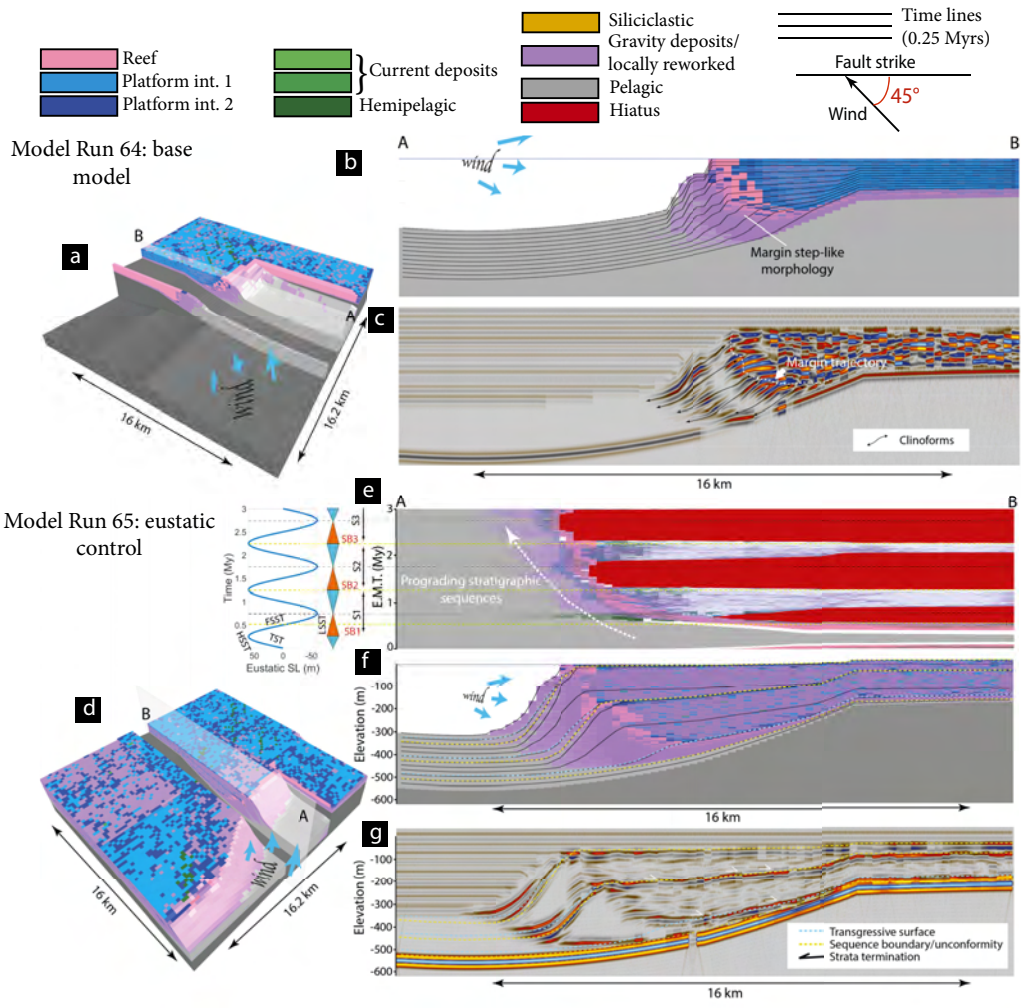
Reef
Platform int. 1
Platform int. 2
Current deposits
Hemipelagic
Siliciclastic
Gravity deposits/
locally reworked
Pelagic
Hiatus
Time lines
(0.25 Myrs)
Fault strike
45°
Wind
Model Run 64: base
model
Model Run 65: eustatic
control
a
b
c
d
e
f
g
A
B
wind
Margin step-like
morphology
Margin trajectory
Clinoforms
16 km
16.2 km
Prograding stratigraphic
sequences
E.M.T. (My)
Time (My)
Eustatic SL (m)
SB3
SB2
SB1
S3
S2
S1
FSST
TST
LST
Elevation (m)
Transgressive surface
Sequence boundary/unconformity
Strata termination

Figure 10 *(previous page)*: Results of *Model run 64-65* showing a sliced 3D view of the models (a, d), a dip-oriented cross-section through each model (b, f), equivalent seismic images of the same cross-section (c, g), and (e), chronostratigraphic diagram of the cross-section from *Model run 65* showing the development of unconformities caused by eustatic sea-level fall. Note the steeped morphology of the transfer zone margins (b and f) generated by long intervals of aggradation, promoted by the highly productive reef factory.

Horst carbonate platforms

Uplifted horsts are structural elements generated by displacement on symmetric, opposing dipping normal faults. In this setting, syn-rift strata are recognizable if the horst is wide enough to show distinct footwall uplift on the flanks and subsidence in between (Dorobek, 2008). CarboCAT modelling results (Figure 11) suggest that the magnitude of this differential subsidence exerts an important control on stratigraphic sequences development and, therefore, on facies heterogeneity.

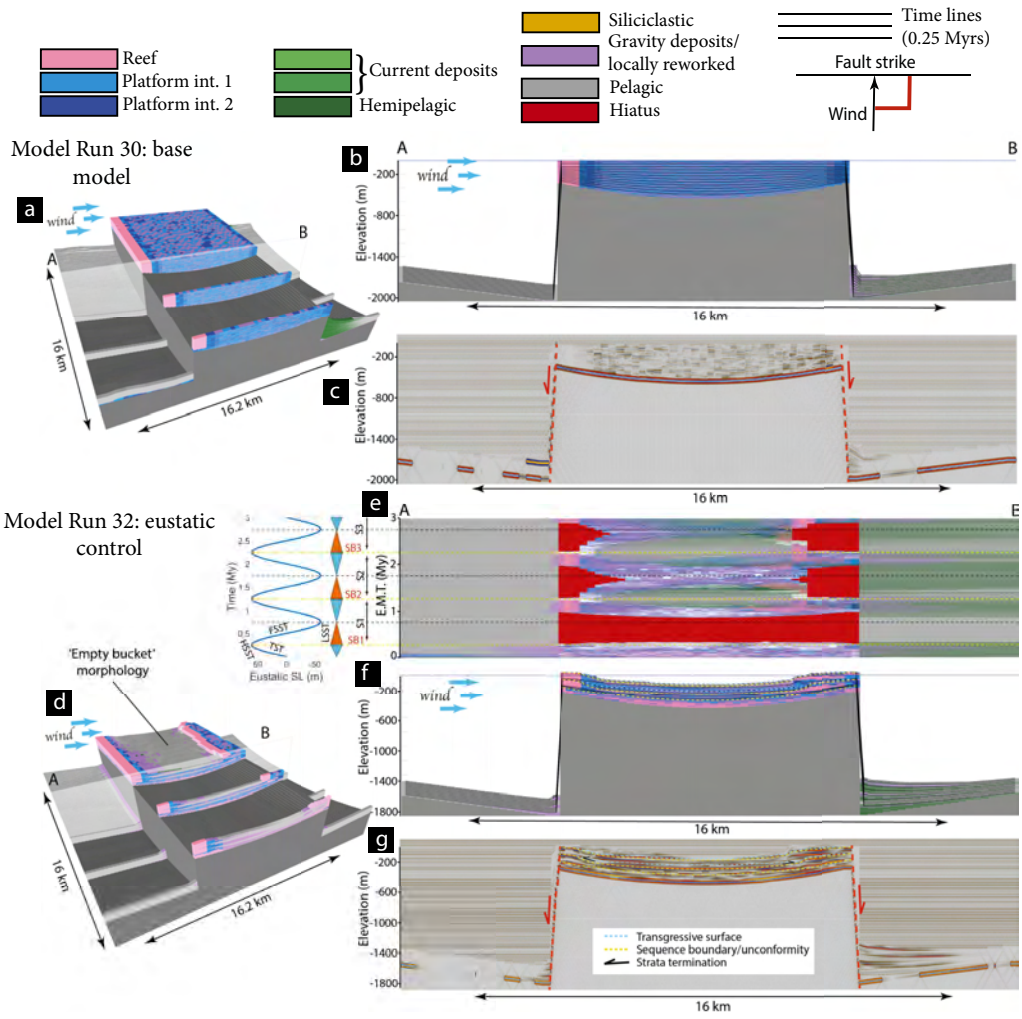
Reef
Platform int. 1
Platform int. 2
Current deposits
Hemipelagic
Siliciclastic
Gravity deposits/ locally reworked
Pelagic
Hiatus
Time lines (0.25 Myrs)
Fault strike
Wind
Model Run 30: base model
Model Run 32: eustatic control
a
b
c
d
e
f
g
wind
A
B
16 km
16.2 km
Elevation (m)
'Empty bucket' morphology
Eustatic SL (m)
Time (My)
E.M.T. (My)
SB1
SB2
SB3
FSST
TST
LSST
Transgressive surface
Sequence boundary/unconformity
Strata termination

Figure 11 *(previous page)*: Results of *Model run 30-32* showing a sliced 3D view of the models (a, d), a dip-oriented cross-section through each model (b, f), equivalent seismic images of the same cross-section (c, g), and (e), chronostratigraphic diagram of the cross-section from *Model run 32* showing the development of unconformities caused by eustatic sea-level fall. Note how increasing subsidence in *Model run 32*, progressively generates accommodation during eustatic sea-level fall events.

Base model - 11 a-c shows the result of *Model run 30*, modelling carbonate growth on horst. Input parameters are listed in Table 3 and include 250 meters of net footwall uplift generating an upward concave depositional surface. This morphology controls deposition of carbonate strata thickening and dipping toward the platform center, with an angle that increases down-section with cumulative fault displacement. Preferential wind direction controls barrier reef development on the windward footwall crest and platform interior strata deposition in the back-reef and leeward footwall crest. Transported sediments are preferentially shed into the leeward basin, developing a thick sedimentary succession. These asymmetries are well-imaged in seismic; the windward platform margin and basin are characterized by acoustically transparent seismic facies, generated by lithologically homogeneous reef and pelagic sediments, respectively. In contrast, the leeward side shows sub-parallel, low amplitude reflection on the footwall crest, generated by acoustic impedance contrast between *Platform interior 1* and *2*, and diverging high-amplitude reflection in the basin. These are generated by the contrast between grainy and fine deposits, which laterally fades toward the pelagic dominated realm.

Eustatic control - *Model run 32* (Figure 11 d-g) has the same input parameters of *Model run 30* but an oscillating sea-level curve (Figure 11 e).

During the first sea-level falling stage and lowstand (stratigraphic sequence S1) the platform top is subaerially exposed for 0.5 My (Figure 11 e). During this period, no platform top carbonate sediments are produced and basin strata are exclusively pelagic. During the subsequent transgressive events, the platform interior progressively drowns, generating a deep lagoon where pelagic and hemipelagic strata are deposited. Meanwhile, reef and platform interior strata keep-up with the rising relative sea-level on the footwall crest, generating a typical asymmetric empty-bucket morphology (*sensu* Schlager, 1981) (Figure 11 d-f). Waves are generated in the lagoon, leading to reefal build-up development on the leeward margin. During S2 and S3 sea-level fall and lowstand, footwall crests are subaerially exposed and the inner platform depositional area is relatively limited, but shallow water controls deposition of thin platform interior strata. During this phase, hanging-wall sedimentation is represented by pelagic and hemipelagic strata alone (Figure 11 e-f). Seismically, composite sequence boundaries and flooding surfaces are marked by highly-negative reflections on the platform margins, generated by highstand platform interior strata burying reef build-ups. Positive reflections on the platform interior are generated by negative acoustic impedance contrast between pelagic and underlying platform interior carbonates (Figure 11 g).

Results discussion and implications

One particularly useful application of experimental numerical stratigraphic forward modelling is to explore the realism and predictive power of existing conceptual models. Constructing and calculating a three-dimensional numerical forward model typically involves a greater level of detail than is

included in many conceptual models, both in the initial conditions that start the model, in the processes included in the model, and in the calculation of synthetic seismic images from the models. Consequently, it is useful to discuss how these forward stratigraphic models of syn-rift and early-post-rift carbonate platforms support and expand or challenge several of the existing conceptual models (e.g. Bosence, 2012; Dorobek, 2008; Cross and Bosence, 2008; Wilson et al., 2000; Burchette, 1988; Leeder and Gawthorpe, 1987), and how that enhances our understanding of how these depositional systems work.

Syn-rift carbonate platform development

Footwall margins

Platform geometry

Fault truncated, aggradational strata characterize the footwall margins of fault block carbonate platforms (e.g. Cross and Bosence, 2008; Burchette, 1988; Leeder and Gawthorpe, 1987). These geometries are controlled by the steep footwall scarp slope, generating a by-pass margin fringed down-slope by a periplatform talus of footwall-derived sediments (Leeder and Gawthorpe, 1987). These field interpretations are supported by stratigraphic model results near the fault center (e.g. *Model Run 1*, 2 and 3; Figure 2 a, d and 4 a). In addition, models illustrate how footwall margin geometry changes along-strike. Near the fault tips, hanging-wall subsidence rate is lower and shallow water carbonates keep-up with base-level rise or prograde from the footwall crest (Figure 10 a and d), burying the fault scarp and terminations. Footwall margin progradation has been described previously by Fabbi and Santanto-

nio (2012) in the Umbria-Marche platform of Central Italy. The presence of in-situ shallow water carbonate in the basins can also occur in land-attached platform settings, where abundant re-sedimentation of footwall-derived siliciclastic sediments forms a shallow substrate (*Model Run 63*; Figure 9 a-b). The timing of transition into a truncated bypass margin is controlled primarily by slip rate exceeding carbonate accumulation in the hanging-wall basins, occurring earlier in fault block platforms characterized by elevated rates of hanging-wall subsidence and low rates of carbonate transport (e.g. compare *Model Run 61* and 64; Figure 3 l and o).

Facies

Shallow-water carbonate platforms commonly dominate the footwall margin of rotated fault blocks, with the development of high-energy facies on wind-facing footwall crests (Burchette, 1988). Low-energy facies in this setting have been related to fault-driven platform margin collapse and exposure of the platform interior facies (Cross and Bosence, 2008). The numerical forward models presented here show that footwall crest stratigraphy can be dominated by low-energy facies originally developed on a flat topography, in a platform interior environment, and then truncated by lateral fault propagation and colonized by reef producers. This ultimately leads to a progressive decrease of reef thickness toward the fault tips (*Model Run 5*; Figure 5 a). Rapid footwall uplift, exceeding regional subsidence and causing emergence, can also prevent the development of high-energy factory near the footwall margin by creating a protected, low-energy area down-dip (*Model Run 23*; Figure 7 a-c).

Stratigraphy

Accommodation near footwall margins is controlled by the interplay of eustatic cycles, regional subsidence and footwall uplift, with the latter expected to control along-strike sequences asymmetries (Leeder and Gawthorpe, 1987). Our new model results support existing model predictions (e.g. Gawthorpe et al., 1994), and highlight the strong control of regional subsidence on stratigraphic development. Although unconformities related to subaerial exposure are common in these settings (e.g. Chow et al., 2013), under constant eustatic sea-level conditions, coseismic footwall uplift exceeding regional subsidence is required (*Model Run 23*; Figure 7 b-c) to uplift the sea floor above sea-level and generate type I sequence boundaries (e.g. Castro Urdiales footwall platform; Rosales et al., 1994). These unconformities are limited to up-dip of the rotation fulcrum (Figure 3 h), and the depositional hiatus is greater at the footwall center, progressively decreasing toward the fault tips where footwall uplift is less pronounced. Under oscillating eustatic sea-level conditions, type I sequences still develop. However, high magnitude glacio-eustatic sea-level falls generate exposure surfaces that can extend well below the rotation fulcrum (*Model Run 2* and *22*; Figure 3 b-g). Transgressive strata are characterized by deposition of reefal build-ups, overlain by highstand platform interior strata. A relatively low regional subsidence rate increases the duration of subaerial exposure events, generating thinner transgressive and highstand units, and allows time equivalent exposure of basinal strata near fault tips (compare *Model Run 2* and *22*; Figure 2 e and 6 e).

Hangingwall margins

Platform geometry

Progradation of the hangingwall dip-slope margin has been frequently associated with phases of decreased fault activity or periods of fault quiescence (e.g. Dorobek, 2008; Wilson et al., 2000). Conversely, backstepping trends are expected when fault-block rotation rate is high (e.g. Cross and Bosence, 2008). Our modelling results suggest that progradation of platform margins on rotating fault blocks is possible, irrespective of slip rate (*Model run 23*; Figure 7 a-d), if high volumes of sediment are redistributed on the platform slope. In contrast, relatively low transport rates generate backstepping (e.g. *Model run 1*; Figure 2 a-b). However, high slip rates do accelerate margin migration rate and the transition into aggradation, particularly near the fault center, (compare *Model run 23* with *Model run 21*, and *Model run 3* with *Model run 21*; Figures 4, 6 and 7) suggesting that extended basinward progradation events on highly rotated dip-slopes may require relative sea-level falls. High slip rates also accelerate the development of a break in slope and consequently, the evolution of the hanging-wall platform from a homoclinal ramp into a step-sided, aggradational shelf (e.g. compare *Model run 1* with *Model run 3*; Figure 2 and 4). This evolutionary trend occurs in all model runs, in agreement with trends described by previous work (e.g. Williams et al., 2011; Barnaby and Read, 1990; Leeder and Gawthorpe, 1987; Read, 1985, 1982).

Facies

The carbonate facies that characterize the hanging-wall dip-slope platform

are largely controlled by the position and orientation of the rotated fault with respect to the rift shoulders, controlling siliciclastic input, and the predominant wind direction. In agreement with the conceptual models proposed by Dorobek (2008), these new modelling results show that low-energy, platform interior facies characterize leeward oriented hanging-wall dip-slopes (e.g. *Model Run 1* and 21, Figure 2 and 6), while windward conditions in this setting control the development of a reefal margin (e.g. *Model Run 4* and *Model Run 24*; Figures 4 and 7). We also demonstrate how the combined effect of relatively high subsidence and rotation rate in this setting can keep the platform margin below the reef factory production depth cut-off, preventing its development until post-rift fault quiescence (*Model run 4*; Figure 4).

Stratigraphy

Ravnås and Steel (1998) and Leeder and Gawthorpe (1987) compared rates of eustatic sea-level changes with displacement rates, concluding that only glacio-eustasy has sufficiently high rates to compete with structurally-driven accommodation changes in synrift settings. Therefore, a continuous rise of relative sea-level is expected in most synrift basins (Gawthorpe et al., 1994) though healthy carbonate platforms should be able to aggrade fast enough to keep up (Schlager, 1981). Some aspects of greenhouse platform margin stacking patterns are retained in sequences generated by eustatic sea-level oscillations (e.g. compare *Model run 1* with 2 and *Model run 21* with *22*; Figure 2 and 6), but vertical and lateral facies heterogeneity is much higher with glacioeustatic forcing and the full range of system tracts are developed (Gawthorpe et al., 1994). Falling stage and lowstand system tracts are

characterized by platform top subaerial exposure and coastline progradation in a forced regression regime, generating wedge-shaped lowstand deposits. During transgressive and highstand stages, the whole system backsteps toward the footwall crest when subsidence rate is relatively high and sediment transport is low. In addition, rotational subsidence progressively reduces coastline regression and smaller, backstepping sequences develop. Progressive lateral decreases of hanging-wall rotation increases subaerial exposure down-dip, toward the fault tips. This effect is less pronounced when low regional subsidence and high transport conditions generate progradational sequences (*Model Run 22* Figure 6) under transgressive and high-stand regimes, leading to hangingwall basin filling and subaerial exposure extending down-dip (compare Figure 3 b and g).

Transfer zones

Platform geometry

Due to the paucity of outcrop analogues and the common practice of interpreting seismic data from along-dip seismic profiles, conceptual models of carbonate platforms developed in transfer zones are rare in literature. Cross and Bosence (2008) expect a progressive steepening of the platform margin controlled by increasing relay ramp rotation, highlighting analogies with hangingwall dip-slope margins. Model results support these hypotheses, but predict a high degree of platform asymmetry in transfer zone settings, controlled by the increase of subsidence rate toward the landward fault plane (see Figure 3 l, o and p). This asymmetric subsidence generates along-dip platform thickening and controls platform margin asymmetric trends (see

Model Run 65; Figure 10 f). Platform margin asymmetry is absent when high in-situ production versus transport rates generate aggradation, locking the platform margin up-dip to the relay ramp (*Model Run 61* and *62*; Figure 8).

Facies

Relay ramps are considered preferred entry point for siliciclastic sediments in the basin (e.g. Gawthorpe and Hurst, 1993). However, when terrigenous input is episodic or absent, the gentle ramp morphology can facilitate carbonate deposition (Gawthorpe and Hurst, 1993; Cross and Bosence, 2008). In more detail, model results suggest that the type of facies that dominates relay ramps is determined by margin migration pattern, which is controlled primarily by transport rates. When aggradation prevails (*Model Run 61* and 62; Figure 8) in-situ carbonate growth is limited to the upper part of the ramp dip-slope, passing downslope to platform-derived resedimented deposits and pelagic facies. Conversely, a shallowing-upward succession can be expected when the platform margin progrades onto older pelagic and slope strata (*Model Run 64* and *65*; Figure 10).

Stratigraphy

Gawthorpe and Hurst (1993) predict that eustatic sea-level changes could dominate the stratigraphy in transfer zones due to the relatively low subsidence. They also expect aggradational and progradational stacking pattern to be facilitated by high sediment supply characterizing these locations. Model results confirm these observations, showing more extended prograda-

tion near ramps than in hanging-wall dip-slope settings when transport rates are high (compare *Model Run 22* with *65*; Figure 6 and 10), and dominant aggradation in low-transport rate systems (compare *Model Run 1* with 61; Figure 2 and 8).

Horst

Platform geometry

Carbonate platform geometry on isolated horsts is influenced by the distance between the two bounding faults. Due to the horizontal wavelength of footwall uplift of approximately 15-20 km (e.g. Stein and Barrientos, 1985), if horst width exceeds 30 km, footwall crest uplift controls the development of strata dipping away from the faults, with a greater angle in older strata due to cumulative displacement generated by multiple uplift events (Dorobek, 2008). These predictions are confirmed by model results (*Model Run 30*; Figure 11). In addition, we illustrate that under glacio-eustatic sea-level oscillation regimes, horst platform morphology closely resembles those developed on atolls (e.g. Warrlich et al., 2002). Rapid sea-level rise forces drowning of the platform interior and the resulting 'empty bucket' morphology (Wright, 1992) is expected to be greater in syn-rift tectonic settings due to the effect of footwall crest uplift (*Model Run 32*; Figure 11).

Facies

Existing models of syn-rift isolated platform on horst highs (i.e. Dorobek, 2011), predict the development of a windward-leeward asymmetry, with high-energy facies developed on the windward footwall crest and the leeward side

dominated by low energy facies. Our models confirm these prediction under constant eustatic sea-level conditions (*Model Run 30*; Figure 11). However, when glacio-eustasy leads to platform interior drowning, waves generated in the lagoon control the development of a high energy margin on the leeward footwall crest (*Model Run 32*; Figure 11).

Stratigraphy

The sub-horizontal morphology of horsts controls the development of an extended area of subaerial exposure (Dorobek, 2008; Ravnås and Steel, 1998) during sea-level falls, resulting in poorly developed low-stand system tracts. Model results illustrate how the development of these sequences is influenced by the increasing differential subsidence occurring between uplifted footwall crests. During early evolutionary stages, this subsidence is low and falling stage and lowstand system tracts are missing. Afterward, cumulative displacement increases accommodation and platform interior strata are generated during sea-level fall and low stand events prior to drowning (Figure 11 e)

Post-rift geometries and stacking patterns

In contrast to siliciclastic systems, where post-rift infill may still be wedge-shaped (Ravnås and Steel, 1998), carbonate platforms tend to develop post-rift subparallel strata (e.g. *Model Run 1* and *21*; Figure 2 and 6). During this phase, the effect of ongoing basin infilling after faulting has ceased may trigger (e.g. *Model Run 21*; Figure 6) or accelerate platform margin progradation near hanging-walls and transfer zones, potentially leading to the coalescence of adjacent platforms, as observed in the South China Sea

by Dorobek (2008). In *Model Run 4* (Figure 4), onset of stable post-rift conditions triggers reef margin deposition.

Controls summary and final remarks

Glacio-eustatic sea-level oscillations

Model results demonstrate that even high-frequency, high-amplitude glacio-eustatic sea-level oscillations only have a minor effect on syn-rift platform morphology in hanging-wall and relay-ramp settings, exacerbating existing platform margin geometries and migration trends rather than forcing new ones. Conversely, the development of empty bucket morphologies on horst is controlled primarily by high rate of sea-level rise, drowning the platform interior (*Model Run 32*; Figure 11), as predicted by the qualitative models of Wright (1992). In addition, icehouse carbonate platforms show greater degree of vertical facies heterogeneity and exposure events that extend below the fault block rotation fulcrum (Leeder and Gawthorpe, 1987), influencing stratigraphy development also in the deepest part of the hanging-wall basins, as previously argued by Gawthorpe et al. (1994).

Antecedent topography and timing of carbonate platform initiation

Timing of carbonate initiation in synrift basins can be hard to determine because flooding can occur at different stages of tectonic development depending on pre-rift topography, amount of stretching (β) and eustatic sea-level (see Dorobek, 2008). These models suggest that early-flooding can be inferred when in-situ carbonate strata are found at the base of synrift successions, proximal to a fault in the hanging-wall basin (e.g. *Model run 1*, Figure 2). In seismic images, these early carbonates may be distinguished

from resedimented deposits by being parallel to the underlying fault block (compare Figure 2 b-c and 6 f-g) and distinguished from lowstand wedges by lack of basin-ward thickening and offlapping geometries (compare Figure 2 b-c and 6 f-g). In addition, lateral fault propagation in existing carbonate strata, typical of fault nucleation rather that reactivation of existing structures, controls the decrease of reef margin thickness toward the tip points (*Model Run 5*; Figure 5 a). In this setting, the development of reef strata is linked to the displacement of existing platform interior strata, exposure of the fault plane and development of high energy conditions. The degree of fault rotation at the time of carbonate initiation also control platform length. High degree of footwall uplift and hanging-wall subsidence, limit the area of the fault block suitable for shallow water carbonate deposition, generating a small, fringing platform (Cross and Bosence, 2008).

Tectonics

Differential subsidence is the primary control on lateral variability of carbonate platforms architecture and facies in extensional settings, regardless of glacio-eustatic sea-level oscillations. Footwall uplift controls the vertical and lateral thickness of carbonate sequences, platform margin geometry and stacking pattern, and the development of subaerial exposure events. In hanging-wall setting, fault block rotation controls platform morphological evolution and the development of typical wedge-shaped strata in cross-section. In addition, along-strike slip rates variation controls platform margin migration trends.

Wind and ecology

In these numerical model experiments, wind direction directly controls reef occurrence and the preferred direction of hemipelagic shedding, in agreement with Dorobek (2008). Wind control tends to fix reef systems in place on the hanging-wall dip-slope platform margin. In this setting, in the absence of other more complex controls, a steep margin characterized by prolonged aggradational stacking throughout the platform history develops. This margin geometry is linked to the lower transport susceptibility of reef strata combined with high accummulation rates, enhancing platform margin vertical growth and reducing sediment supply to the adjacent slope. The control on platform morphology by carbonate transportability has been qualitatively argued previously (Adams and Schlager, 2000; Kenter, 1990) and supported using a 2D numerical modelling approach by Williams et al. (2011). The relationship between the amount of carbonate accumulated in-situ and the volume shed into the adjacent basin represents a primary control on platform morphology and stacking pattern in hanging-wall and transfer zone margins.

Recommendations

Our model results illustrate again the dramatic effect that different carbonate factories with different transportability and rates of in-situ growth can have on platform development. Therefore, understanding and predicting ecological variability of carbonate-producing organisms and accommodation (Pomar and Hallock, 2008) is essential for a correct interpretation of carbonate platform architecture and facies heterogeneity. Development of numerical models to explore this further would be useful. In addition, this study demonstrates

that a detailed interpretation of structurally controlled platform geometries in three-dimension is required in extensional basins, to correctly predict variability of platform thickness, the lateral extent of facies, and subaerial exposure with the ultimate aim of predicting geobody volume and connectivity. To make progress with this, quantitative metrics are required that can be applied to 3D model output to define, characterise and rigorously compare the stratal geometries present.

Seismic signatures

Carbonate strata heterogeneity in seismic images is controlled by a wide spectrum of parameters including variability in strata architecture (e.g. Sarg, 1988), petrophysical properties (e.g. Ehrenberg et al., 2006), diagenetic overprint (e.g. Jones and Xiao, 2006) and structural deformation (e.g. Yose et al., 2001). Addressing this entire range of complexity in our synthetic seismic modelling to account for every possible case is not possible. However, these synthetic seismic images do show stratal geometries and heterogeneity comparable with observed seismic images of carbonate strata (e.g. Rankey et al., 2019; Fournier et al., 2005). Therefore, some general observations are possible based on these results, to guide which geological elements are or are not seismic resolvable and how they are imaged.

Carbonate platform architecture is the main control on seismic geometries (e.g. Eberli et al., 2004; Kleipool et al., 2017). Seismic modelling results illustrate how backstepping platform margin developed on highly rotated hanging-wall and relay-ramp dip slopes can be identified in seismic by abrupt changes in reflector dips, defining sigmoidal geometries, rather than polarity or amplitude changes. Numerous platform top reflectors (e.g. *Model Run 4*

and 3) show good continuity and constant polarity and amplitude when passing into slope margin facies. These events do not reflect the underlying facies variability, and the onlapping strata termination against the steeply dipping platform margin. Conversely, when the underlying strata are controlled by relative sea-level oscillations, rather extreme vertical and lateral facies transitions generate higher acoustic impedance contrasts. Hanging-wall platform margins are defined by the transition between high amplitude platform top facies and rather transparent pelagic sediment. Sequence boundaries in backstepping systems are marked by reflection between platform interior strata and overlying transgressive basinal facies, while prograding systems are imaged by a peak at the transition between high-stand and transgressive deposits. In these systems, relatively high fault block rotation generates abrupt bathymetric difference between the platform margin and the adjacent basin. Fringing aprons are imaged by relatively high-amplitude reflectors, generated by the high acoustic impedance contrast between coexisting relatively low porosity hemipelagic sediments and high porosity gravity deposits. In contrast, prograding hanging-wall margins over more gentler hanging-wall dip-slopes are characterized by a gradual transition from the high-amplitude, high-frequency platform-top facies to relatively transparent sigmoidal slope facies, dominated by gravity flow deposits. Hemipelagic facies deposition occurs only in the distal slope, where the bathymetry is below the wave base. Here, alternating hemipelagic, pelagic and gravity deposits generate high amplitude, high frequency seismic reflections. Footwall margins are characterized by aggradational stacking of single facies with uniform elastic properties, resulting in a transparent seismic facies. Here, internal reflections

are generated only when glacio-eustatic sea-level oscillations control vertical stacking of high-energy reef strata and platform interior during high-stands.

In these simple models the base of carbonate platform strata is imaged as a continuous, high-amplitude negative reflector, generated by the high acoustic impedance contrast between carbonates and underlying siliciclastic strata. In contrast, the top carbonate reflection shows lateral variation in polarity and amplitude, reflecting underlying carbonate heterogeneity. A similar contrast between platform top and bottom carbonate has been observed in some real carbonate build-ups. For example, the Malampaya build-up (offshore Philippines) shows a continuous, high-amplitude bottom reflection and a carbonate top represented, on the eastern platform top and margin, by an envelope of reflection terminations showing polarity changes (Burgess et al., 2013; Fournier et al., 2005, 2004).

Conclusions

Syn-rift carbonate platforms are complex, and our understanding of how such carbonate strata may develop remains incomplete. Analysis of CarboCAT numerical stratigraphic forward models of syn-rift carbonate strata confirms some key elements of existing conceptual models, but also expand our knowledge of how these depositional systems work, suggesting that some important additions and modifications are required.

- Modelled carbonate strata deposited in horst, half-graben and transfer zone settings successfully reproduce the fundamental platform morphologies and facies distributions character described in existing con-

ceptual models and outcrop-based studies (e.g. Bosence, 2012; Williams et al., 2011; Dorobek, 2011; Cross and Bosence, 2008; Wilson et al., 2000; Leeder and Gawthorpe, 1987) suggesting that both the conceptual and the numerical model formulations are reasonable, and the input parameter values used in these numerical models are appropriate.

- Footwall margin carbonate platforms are characterised by fault-truncated carbonate strata near the fault centre. Near the fault tips, decreasing subsidence rates encourage footwall margin progradation into the hanging-wall basin. Accommodation in this setting is controlled primarily by regional subsidence and eustatic sea-level oscillations, with footwall uplift controlling lateral sequences asymmetry. Compared to existing conceptual models, we have demonstrated how fault propagation may control the lateral variability of carbonate facies near footwall margins where high-energy facies may colonize platform interior area after being fault truncated. This further emphasizes that detailed fault timing constraints are required to properly characterize facies heterogeneity in this setting. The observed vertical facies transition may be recognized in subsurface data by seismic facies transition into more continuous reflectors characterizing platform interior strata.

- Hanging-wall carbonate strata are characterised by growth patterns. In these setting, slip rate controls evolution of the platform from a homoclinal ramp into a flat-topped, steep-margin platform. Our model demonstrates that hanging-wall stacking patterns are primarily con-

trolled by the rate of sediment redistribution into the adjacent slopes. Under high-transport regimes the platform is likely to prograde down-dip. In low-transport systems the platform margin quickly backsteps toward the footwall crest. These different margin geometries control slope re-sedimentation and generate distinctive seismic motifs.

- Transfer-zone carbonate strata show similarities with those developed near hanging-wall margins; sediment transport regime is the primary control on platform margin stacking pattern, and platforms always tend to evolve over time into flat-top steep-margin platform. However, model results predict that relay-ramp strata are characterized by a higher degree of asymmetry, controlled by tilting generating along-dip thickening.

- Horst carbonate strata geometries are controlled by the distance between the two bounding faults. If horst width exceeds $30km$, symmetric footwalls uplift generates growth strata dipping away from both faults. Similarly to atoll settings, icehouse eustatism generates empty bucket morphologies, accentuated in this setting by symmetric footwall uplift. Model results show how facies development near the leeward footwall crest may be affected by waves generated in the platform interior.

- Synthetic seismic images of CarboCAT model results are comparable with observed seismic images of carbonate strata in terms of imaged platform geometries, reflection continuity, and seismic facies heterogeneity. Interesting features developed in these seismic images include the control on platform margin imaging by hanging-wall platform stack-

ing patterns. Prograding platforms on gentle dip-slopes are characterized by gradual facies transition from platform interior to slope grainy facies and distal hemipelagic and pelagic. Each of this platform elements generates a distinct seismic facies resulting in a well defined platform margin. Conversely, backstepping platforms develop bypass slopes with fringing aprons where grainy sediments are mixed with fine-grained facies generating continuous high amplitude seismic reflections from the platform interior onto the slope. This could make platform margin identification more challenging.

- These first results from analysis and comparison of synthetic seismic images suggest that there is significant potential for follow-on work to explore in more detail how external controlling factors in carbonate depositional systems lead to specific seismic image features.

Acknowledgements

Isabella Masiero would like to acknowledge financial support from Tullow Oil, Woodside Petroleum, and Wintershall. The authors thank NORSAR Innovation AS for the academic use of SeisRoX to create synthetic seismic images, and Schlumberger for use of Petrel software. Erwin Adams, Jim Hendry and an anonymous reviewer are thanked for the suggestions and comments that improved the final version of this publication.

References

Adams, E.W. and Schlager, W., 2000. Basic Types of Submarine Slope Curvature. *Journal of Sedimentary Research*, **70**, 814–828. URL http://dx.doi.org/10.1306/2dc4093a-0e47-11d7-8643000102c1865d

Anselmetti, F.S. and Eberli, G.P., 1993. Controls on sonic velocity in carbonates. *Pure and Applied Geophysics*, **141**, 287–323. URL http://dx.doi.org/10.1007/BF00998333

Barnaby, R.J. and Read, J.F., 1990. Carbonate ramp to rimmed shelf evolution: Lower to Middle Cambrian continental margin, Virginia Appalachians. *Geological Society of America Bullettin*, **102**, 391–404. URL http://dx.doi.org/10.1130/0016-7606(1990)102<0391:CRTRSE>2.3.CO;2

Bosence, D., 2012. Carbonate-dominated marine rifts. *In:* David, G. and Bally, A. (eds.) *Regional Geology and Tectonics: Phanerozoic Rift Systems and Sedimentary Basins*, 78. Elsevier B.V., 104–130. URL http://dx.doi.org/10.1016/B978-0-444-56356-9.00005-5

Bosence, D., Cross, N. and Hardy, S., 1998. Architecture and depositional sequences of Tertiary fault-block carbonate platforms; an anlysis from outcrop (Miocene, Gulf of Suez) and computer modelling. *Marine and Petroleum Geology*, **15**, 203–221. URL http://dx.doi.org/10.1016/S0264-8172(98)00016-6

Bosworth, W., Crevello, P., Winn, R. and Steinmetz, J., 1998. Structure, sedimentation, and basin dynamics during rifting of the Gulf of Suez and

north-western Red Sea. *In:* Purser, B. and Bosence, D. (eds.) *Sedimentation and Tectonics in Rift Basins Red Sea:-Gulf of Aden*, 78. Springer, 77–96

Burchette, T.P., 1988. Tectonic control on carbonate platform facies distribution and sequence development: Miocene, Gulf of Suez. *Sedimentary Geology*, **59**, 179–204

Burgess, P.M., 2013. CarboCAT: A cellular automata model of heterogeneous carbonate strata. *Computers & Geosciences*, **53**, 129–140

Burgess, P.M., Winefield, P., Minzoni, M. and Elders, C., 2013. Methods for identification of isolated carbonate buildups from seismic reflection data. *AAPG Bulletin*, **97**, 1071–1098. URL `http://dx.doi.org/10.1306/12051212011`

Chow, N., George, A.D., Trinajstic, K.M. and Chen, Z.Q., 2013. Stratal architecture and platform evolution of an early Frasnian syn-tectonic carbonate platform, Canning Basin, Australia. *Sedimentology*, **60**, 1583–1620. URL `http://dx.doi.org/10.1111/sed.12041`

Cowie, P.A. and Scholz, C.H., 1992. Displacement-length scaling relationship for faults: data synthesis and discussion. *Journal of Structural Geology*, **14**, 1149–1156. URL `http://dx.doi.org/10.1016/0191-8141(92)90066-6`

Cross, N.E. and Bosence, D., 2008. Tectono-sedimentary models for rift-basin carbonate systems. *In:* Lukasik, J. and Simo, T. (eds.) *Controls on Carbonate Platform and Reef Development, SEPM, Special Publication*, 89. 83–105

Dorobek, S., 2008. Tectonic and depositional controls on syn-rift carbonate platform sedimentation. *In:* Lukasik, J. and Simo, T. (eds.) *Controls on Carbonate Platform and Reef Development, SEPM, Special Publication*, 89. 57–81

Eberli, G.P., Masaferro, J.L. and Sarg, J.F., 2004. Seismic imaging of carbonate reservoirs and systems. *In:* Eberli G.P., Masaferro J.L., S.J. (ed.) *Seismic imaging of carbonate reservoirs and systems*, 81. AAPG Memoir, Tulsa, OK, 1–9

Ehrenberg, S.N., Eberli, G.P. and Baechle, G., 2006. Porosity-permeability relationships in Miocene carbonate platforms and slopes seaward of the Great Barrier Reef, Australia (ODP Leg 194, Marion Plateau). *Sedimentology*, **53**, 1289–1318. URL `http://dx.doi.org/10.1111/j.1365-3091.2006.00817.x`

Enos, P., 1991. Sedimentary parameters for computer modeling. *Kansas Geological Survey, Bulletin*, **233**, 63–99

Fabbi, S. and Santantonio, M., 2012. Footwall progradation in syn-rift carbonate platform-slope systems (Early Jurassic, Northern Apennines, Italy). *Sedimentary Geology*, **281**, 21–34. URL `http://dx.doi.org/10.1016/j.sedgeo.2012.07.008`

Fournier, F., Borgomano, J. and Montaggioni, L.F., 2005. Development patterns and controlling factors of Tertiary carbonate buildups: Insights from high-resolution 3D seismic and well data in the Malampaya gas field

(Offshore Palawan, Philippines). *Sedimentary Geology*, **175**, 189–215. URL http://dx.doi.org/10.1016/j.sedgeo.2005.01.009

Fournier, F., Léonide, P., Kleipool, L., Toullec, R., Reijmer, J.J., Borgomano, J., Klootwijk, T. and Van Der Molen, J., 2014. Pore space evolution and elastic properties of platform carbonates (Urgonian limestone, Barremian-Aptian, SE France). *Sedimentary Geology*, **308**, 1–17. URL http://dx.doi.org/10.1016/j.sedgeo.2014.04.008

Fournier, F., Montaggioni, L. and Borgomano, J., 2004. Paleoenvironments and high-frequency cyclicity from Cenozoic South-East Asian shallow-water carbonates: A case study from the Oligo-Miocene buildups of Malampaya (Offshore Palawan, Philippines). *Marine and Petroleum Geology*, **21**, 1–21. URL http://dx.doi.org/10.1016/j.marpetgeo.2003.11.012

Gawthorpe, R.L., Fraser, A.J. and Collier, R.E., 1994. Sequence stratigraphy in active extensional basins: implications for the interpretation of ancient basin-fills. *Marine and Petroleum Geology*, **11**, 642–658. URL http://dx.doi.org/10.1016/0264-8172(94)90021-3

Gawthorpe, R. and Hurst, J.M., 1993. Transfer zones in extensional basins: their structural style and influence on drainage development and stratigraphy. *Journal of the Geological Society*, **150**, 1137–1152

Jackson, J. and McKenzie, D., 1988. Rates of active deformation in the Aegean Sea and surrounding regions. *Basin Research*, **1**, 121–128. URL http://dx.doi.org/10.1111/j.1365-2117.1988.tb00009.x

Jones, G.D. and Xiao, Y., 2006. Geothermal convection in the Tengiz carbonate platform, Kazakhstan: Reactive transport models of diagenesis and reservoir quality. *AAPG Bulletin*, **90**, 1251–1272. URL http://dx.doi.org/10.1306/04030605194

Kenter, J., 1990. Carbonate platform flanks : slope angle and sediment fabric. *Sedimentology*, **37**, 777–794

Kleipool, L.M., de Jong, K., de Vaal, E.L. and Reijmer, J.J., 2017. Seismic characterization of switching platform geometries and dominant carbonate producers (Miocene, Las Negras, Spain). *Sedimentology*, **64**, 1676–1707. URL http://dx.doi.org/10.1111/sed.12369

Lecomte, I., 2008. Resolution and illumination analyses in PSDM: A ray-based approach. *The Leading Edge*, **27**, 650–663. URL http://dx.doi.org/10.1190/1.2919584

Lecomte, I., Lavadera, P.L., Anell, I., Buckley, S.J., Schmid, D.W. and Heeremans, M., 2015. Ray-based seismic modeling of geologic models: Understanding and analyzing seismic images efficiently. *Interpretation*, **3**, SAC71–SAC89

Leeder, M.R. and Gawthorpe, R.L., 1987. Sedimentary models for extensional tilt-block/half-graben basins. *In:* Coward M.P., Dewey J.F., H.P. (ed.) *Continental Extensional Tectonics*, 28. 139–152. URL http://dx.doi.org/10.1144/GSL.SP.1987.028.01.11

Loza Espejel, R., Alves, T.M. and Blenkinsop, T.G., 2019. Distribution and growth styles of isolated carbonate platforms as a function of fault

propagation. *Marine and Petroleum Geology*, **107**, 484–507. URL http://dx.doi.org/10.1016/j.marpetgeo.2019.05.020

Mandlier, P.G. and Kench, P.S., 2012. Analytical modelling of wave refraction and convergence on coral reef platforms: Implications for island formation and stability. *Geomorphology*, **159-160**, 84–92. URL http://dx.doi.org/10.1016/j.geomorph.2012.03.007

Masiero, I., Kozlowski, E., Antonatos, G., Xi, H. and Burgess, P., 2020. Numerical stratigraphic forward models as conceptual knowledge repositories and experimental tools: An example using CarboCAT new version. *Computers & Geosciences*, **138**, 129–140

Miall, A.D., 2010. *The geology of stratigraphic sequences*. 304 pp. Springer, Berlin, Heidelberg

Miller, K.G., Kominz, M.A., Browning, J.V., Wright, J.D., Mountain, G.S., Katz, M.E., Sugarman, P.J., Cramer, B.S., Christie-Blick, N. and Pekar, S.F., 2005. The Phanerozoic record of global sea-level change. *Science*, **310**, 1293–1298. URL http://dx.doi.org/10.1126/science.1116412

Morley, C.K., Nelson, R.A., Patton, T.L. and Munn, S.G., 1990. Transfer zones in the East African Rift System and their relevance to hydrocarbon explorationin rifts. *AAPG Bulletin*, **74**, 1234–1253

Péquignet, A.C., Becker, J.M., Merrifield, M.A. and Boc, S.J., 2011. The dissipation of wind wave energy across a fringing reef at Ipan, Guam. *Coral Reefs*, **30**, 71–82. URL http://dx.doi.org/10.1007/s00338-011-0719-5

Perrin, C., Plaziat, J.C. and Rosen, B., 1998. Miocene coral reefs and reef corals of the south-western Gulf of Suez and north-western Red Sea: distribution, diversity and regional environmental controls. *In:* Purser, B. and Bosence, D. (eds.) *Sedimentation and Tectonics in Rift Basins Red Sea:-Gulf of Aden*, 78. Springer, Dordrecht, Netherlands, 296–319

Playton, T. and Kerans, C., 2002. Slope and Toe-of-Slope Deposits Shed from a Late Wolfcampian Tectonically Active Carbonate Ramp Margin. *Gulf Coast Association of Geological Societies Transactions,*, **52**, 811–820

Pomar, L. and Hallock, P., 2008. Carbonate factories: A conundrum in sedimentary geology. *Earth-Science Reviews*, **87**, 134–169. URL `http://dx.doi.org/10.1016/j.earscirev.2007.12.002`

Purkis, S.J., Harris, P.M. and Ellis, J., 2012. Patterns of sedimentation in the contemporary Red Sea as an analog for ancient carbonates in rift settings. *Journal of Sedimentary Research*, **82**, 859–870

Purser, B., Barrier, P., Montenat, C., Orszag-Sperber, F., DEstevou, P.O., Plaziat, J.C. and Philobbos, E., 1998. Carbonate and siliciclastic sedimentation in an active tectonic setting: Miocene of the north-western Red Sea rift, Egypt. *In:* Purser, B. and Bosence, D. (eds.) *Sedimentation and Tectonics in Rift Basins Red Sea:-Gulf of Aden*, 78. Springer: Dordrecht, Netherlands, 239–270

Rankey, E.C., Schlaich, M., Mokhtar, S., Ghon, G., Ali, S.H. and Poppelreiter, M., 2019. Seismic architecture of a Miocene isolated carbonate platform and associated off-platform strata (Central Luconia Province,

offshore Malaysia). *Marine and Petroleum Geology*, **102**, 477–495. URL http://dx.doi.org/10.1016/j.marpetgeo.2019.01.009

Ravnås, R. and Steel, R.J., 1998. Architecture of marine rift-basin successions. *AAPG Bulletin*, **82**, 110–146. URL http://dx.doi.org/10.1306/1d9bc3a9-172d-11d7-8645000102c1865d

Read, J.F., 1982. Carbonate platforms of passive (extensional) continental margins: Types, characteristics and evolution. *Tectonophysics*, **81**, 195–212. URL http://dx.doi.org/10.1016/0040-1951(82)90129-9

Read, J.F., 1985. Carbonate Platform Facies Models. *AAPG Bulletin*, **69**, 1–21. URL http://dx.doi.org/10.1306/ad461b79-16f7-11d7-8645000102c1865d

Roberts, H.H. and Murray, S.P., 1984. Developing carbonate platforms: southern Gulf of Suez, northern Red Sea. *Marine Geology*, **59**, 165–185

Rosales, I., 1999. Controls on carbonate-platform evolution on active fault blocks; the Lower Cretaceous Castro Urdiales Platform (Aptian-Albian, northern Spain). *Journal of Sedimentary Research*, **69**, 447–465

Rosales, I., Fernandez-Mendiola, P.A. and Garcia-Mondejar, J., 1994. Carbonate depositional sequence development on active fault blocks: the Albian in the Castro Urdiales area, northern Spain. *Sedimentology*, **41**, 861–882. URL http://dx.doi.org/10.1111/j.1365-3091.1994.tb01429.x

Rosendahl, B.R., 1987. Architecture of continental rifts with special reference to east Africa. *Annual Review of Earth and Planetary Sciences*, **15**, 445–503

Rosendahl, B., Reynolds, D., Lorber, P., Burgess, C., McGill, J., Scott, D., Lambiase, J. and Derksen, S., 1986. Structural expressions of rifting: lessons from Lake Tanganyika, Africa. *In:* Frostick, L. and Reid, I. (eds.) *Sedimentation in the African Rifts*, 25. Geological Society of London, 29–43

Schlager, W., 1981. The paradox of drowned reefs and carbonate platforms. *Geological Society of America Bulletin*, **92**, 197–211

Schlager, W., 2000. Sedimentation rates and growth potential of tropical, cool-water and mud-mound carbonate systems. *In:* Insalaco, E., Skelton, P. and Palmer, T. (eds.) *Carbonate platform systems: components and interactions*, 178. Geological Society of London, 217–227

Schlager, W., Reijmer, J.J.G. and Droxler, A., 1994. Highstand Shedding of Carbonate Platforms. *Journal of Sedimentary Research*, **64**, 270–281. URL `http://dx.doi.org/10.1306/D4267FAA-2B26-11D7-8648000102C1865D`

Stein, R.S. and Barrientos, S.E., 1985. Planar High-Angle Faulting in the Basin and Range' Geodetic Analysis of the 1983 Borah Peak, Idaho, Earthquake. *Journal of Geophysical Research*, **90**, 355–366

Warrlich, G.M., Waltham, D.A. and Bosence, D.W., 2002. Quantifying the sequence stratigraphy and drowning mechanisms of atolls using a new 3-D forward stratigraphic modelling program (CARBONATE 3D). *Basin Research*, **14**, 379–400. URL `http://dx.doi.org/10.1046/j.1365-2117.2002.00181.x`

Williams, H.D., Burgess, P.M., Wright, V.P., Della Porta, G. and Granjeon, D., 2011. Investigating Carbonate Platform Types: Multiple Controls and a Continuum of Geometries. *Journal of Sedimentary Research*, **81**, 18–37. URL http://dx.doi.org/10.2110/jsr.2011.6

Wilson, M.E., Bosence, D.W. and Limbong, A., 2000. Tertiary syntectonic carbonate platform development in Indonesia. *Sedimentology*, **47**, 395–419. URL http://dx.doi.org/10.1046/j.1365-3091.2000.00299.x

Wright, V.P., 1992. Speculations on the controls on cyclic peritidal carbonates: ice-house versus greenhouse eustatic controls. *Sedimentary Geology*, **76**, 1–5. URL http://dx.doi.org/10.1016/0037-0738(92)90135-E

Yose, L.A., Eiben, T., Brown, S., Kompanik, G.S., Davis, T.L. and Maxwell, S.R., 2001. 3-D geologic model of a fractured carbonate reservoir, Norman Wells Field, NWT, Canada. *Bulletin of Canadian Petroleum Geology*, **49**, 86–116. URL http://dx.doi.org/10.2113/49.1.86